C.P. No. 1157

C.P. No. 1157

MINISTRY OF AVIATION SUPPLY

AERONAUTICAL RESEARCH COUNCIL

CURRENT PAPERS

Induced Rolling Moment Characteristics of the M557A Streamline Bomb at Mach Number 0.50

by

P. Lee and I. G. Hacker

Aerodynamics Dept., R.A.E., Farnborough

LONDON: HER MAJESTY'S STATIONERY OFFICE

1971

PRICE 80p NET

CP No.1157*
July 1969

INDUCED ROLLING MOMENT CHARACTERISTICS OF THE M557A STREAMLINE BOMB AT MACH NUMBER 0.50

by

P. Lee
I. G. Hacker
Aerodynamics Department, R.A.E., Farnborough

SUMMARY

A model of a streamline bomb with fixed cruciform fins has been tested in the R.A.E. 8 ft × 6 ft tunnel, to examine possible reasons for the discrepancy between the rolling moments derived from free flight tests and results obtained from previous wind tunnel tests.

A range of Reynolds numbers was covered corresponding to the previous tunnel test and free flight values. The effect on rolling moment of a nose probe and a launching lug, which were present in the flight tests but not represented in the previous tunnel tests, also was investigated.

The results show that the induced rolling moment was not significantly influenced by Reynolds number, for the range covered. At incidence a large change in rolling moment resulted for the addition of the nose probe and it was shown that this rolling moment depended critically on the geometric accuracy of the spherical nose of the probe itself.

---

*Replaces R.A.E. Technical Memorandum Aero 1154 - ARC 31839

CONTENTS

1 INTRODUCTION

Ref.1 gives details of free flight and wind tunnel tests on bombs stabilised by fixed cruciform fins. The comparisons of flight and tunnel measurements, given in this reference, for a streamline bomb designated M557A, show that although in general there is good agreement for the normal force and restoring moment, the induced rolling moments derived from the flight data differ considerably from the moments measured in the tunnel tests.

This poor comparison of flight and tunnel rolling moments is a serious obstacle to the accurate prediction of the flight dynamic behaviour of bombs, using data derived from tunnel tests, as the magnitude of the rolling moment has a large influence on the initial behaviour of bombs at release and can result in roll lock in[2] and catastrophic yawing behaviour.

The test made in the R.A.E. 8 ft × 6 ft wind tunnel on M557A at a Mach number 0.50 (the flight Mach number at release), reported in this paper were made to investigate in detail the variation of rolling moment with model attitude and to examine possible reasons for the differences between the induced rolling moments measured in flight and in the tunnel.

The tests were made in two parts. In the first series of tests (March 1967) the effect of Reynolds number on induced rolling moment was investigated. The range of Reynolds number covered varied from that of the previous tunnel tests to the full scale value at M = 0.50. In the second series (June 1967), the effects of the launching lug and yawmeter nose probe on rolling moment were examined. These items were present on the free flight bombs but not represented in the previous tunnel tests.

2 MODEL DETAILS

The bomb model M557A used for the first series of tests was the same model, unmodified, as tested in the A.R.A. tunnel and reported in Ref.1. A dimensioned drawing of the bomb is given in Fig.1. Prior to the second series of tests the first two inches of the nose section of the model was removed and two alternative replacement noses were manufactured. One of these represented the nose of the bomb with the yawmeter probe in position (Fig.2) as used in the flight tests, when the induced rolling moment was measured. The other nose was nominally identical to the original pointed nose. This replacement pointed nose was used as the datum condition for the second series of tests. A further modification to the model was also made so that the launching lug used in the flight tests could be represented on the model.

A new five component strain gauge balance was used for all these tests, the original balance not having sufficient load capacity for the tests at the higher Reynolds numbers. The geometry of the exposed portion of this replacement sting balance differed slightly from that of the original sting. The included angle of the sting at the base of the model being 5.75 degrees for the new sting compared with 4.5 degrees for the original sting.

3 EXPERIMENTAL DETAILS

The first series of tests were made in the 8 ft × 6 ft tunnel with a solid wall working section configuration, this type of working section was used as the tests were made during a break in a test programme on two-dimensional aerofoils for which the working section had been extensively modified. The second series of tests were made with the standard 8 ft × 6 ft slotted working section, open area ratio 10%.

Measurements were made of the normal force Z, pitching moment m, side force Y, yawing moment n and rolling moment l acting on the model for the configurations, Reynolds numbers and model attitude ranges listed in Tables 1 and 2. For all the test conditions boundary layer transition was allowed to occur naturally on both the body and the fins. The measured forces and moments were resolved to give the forces and moments in and normal to the plane of the total incidence angle. Fig.3 gives the axis and sign convention used. The moment reference point used was at 0.5 × the body length aft of the nose. In reducing the data to coefficient form the maximum body diameter (11.91 cm) and cross sectional area (111.33 cm^2) were used as the reference length and area.

The probable accuracy of the measured loads in coefficient form is estimated to be:-

C_z', C_y' : ±0.02

C_m', C_n' : ±0.02

C_l : ±0.001.

In making these estimates no account has been taken of the possible influence on the aerodynamic loads, of geometric inaccuracies of the model. It can be seen from the results that differences greater than the estimated accuracy exist between geometrically identical conditions i.e. σ, λ and σ, $\lambda \pm 90$, and that these differences are most apparent in the case of rolling moment.

Angular settings of the model were corrected for sting and balance deflection and a correction has been made to allow for the small downwash of the tunnel airstream at the model location. The results were not corrected for tunnel constraint or blockage as these corrections were considered to be negligible. The validity of this assumption is shown by Fig.17, the variation of normal force with incidence being almost identical for both the solid (first series of tests) and slotted (second series of tests) wall working section configurations.

In order to aid the understanding of the results flow visualization studies were made at $\sigma = 20^{\circ}$, $\lambda = 22.5$ and $\sigma = 16^{\circ}$, $\lambda = 17.5$ for the model with the original pointed nose and at $\sigma = 20^{\circ}$, $\lambda = 0^{\circ}$ for the model with and without the nose probe in position.

4 PRESENTATION OF RESULTS

The principle results for both series of tests are presented graphically in Figs.4-15 and 17-27. For convenience in Figs.4, 5, 8 and 9 the results for roll angles greater than 90° are shown as the data for the negative incidence range of the appropriate curves for roll angles less than 90°.

Figs.6, 7, 10, 11 and 14 show the variation of C_z', C_m' C_y', C_n' and C_l with incidence at a constant roll angle for the model with the original pointed nose at Reynolds numbers, based on body diameter, of 1.29×10^6, 1.92×10^6 and 2.60×10^6. In a similar manner Figs.17, 18, 19, 20 and 24 give the results for all the configurations tested, including the original and replacement pointed noses at a Reynolds number of 1.29×10^6.

The variation of rolling moment with roll angle at a constant incidence is given for the original configuration in Fig.15 and for the configurations tested in the second series of tests in Figs.25, 26 and 27. A selection of the side force and yawing moment data measured in these runs is presented in Figs.12, 21, 22 and 23. None of the normal force and pitching moment data measured during these runs is given as it is considered that the variation of C_z' and C_m' with roll angle is adequately defined by the data given in Figs.4, 5, 17 and 18. The pictures obtained in the flow visualization tests mentioned in section 3 are shown in Figs.16 and 28.

5 DISCUSSION OF RESULTS

This section is mainly restricted to a discussion of the measurements of rolling moment. The general aerodynamic characteristics of the bomb are fully discussed in detail in Ref.1.

5.1 Effects of Reynolds number on original pointed nose configuration

It can be seen from Fig.14 that increasing Reynolds number from 1.29×10^6 to 2.6×10^6 has a small measurable effect on the rolling moment acting on the model, the largest differences occurring at the highest test incidence $\sigma = 20^\circ$, and are of the order of $\Delta Cl = 0.04$ to 0.09. The other components are almost uninfluenced by this change of Reynolds number (Figs.6, 7, 10 and 11).

The magnitude of the changes of rolling moment coefficient with increasing Reynolds number does not however, significantly alter the variation of C_l with incidence. From Fig.14 it can be seen that at $\lambda = 22.5^\circ$ the rolling moments measured at all the test Reynolds numbers largely confirm the previous tunnel results. Both sets of results show that at $\lambda = 22.5^\circ$ increasing incidence from zero causes initially a negative rolling moment but at approximately 15° this trend is reversed and there is a rapid positive rise of rolling moment.

The differences between the flight and previous tunnel tests are therefore not directly attributable to scale effect.

5.2 Variation of rolling moment with roll angle for incidences $\geq 12^\circ$ for the original pointed nose

Fig.15 shows the variation of rolling moment with roll angle over a complete roll revolution and it can be seen from this figure that at $\sigma = 20^\circ$ the variation is approximately sinusoidal as expected, although the peak values of the rolling moment differ considerably in the various quadrants. As the incidence is reduced from 18° to 14° a phase change of approximately 45° occurs in the variation of C_l with roll angle.

Fig.16 shows the flow patterns formed on the fins at $\sigma = 20^\circ$, $\lambda = 22.5$ and $\sigma = 16^\circ$, $\lambda = 27.5^\circ$, these settings corresponding to peak positive and negative values in the C_l V_s λ curves. From these pictures it is apparent that the interaction of the body vortices with the fins give rise to flow which is extremely complex. The main difference between these two conditions is, however, that at $\sigma = 20^\circ$ (Fig.16a) the interaction of the body vortices with the fins results in the flow over the upper surface of the port fin being mainly separated whilst at $\sigma = 16^\circ$ (Fig.16b) the flow over the upper surface of the starboard fin is separated. This switching of the separated flow regions from the starboard to port fins as the incidence is

increased is most probably the primary reason for the rolling moment being initially negative as the incidence is increased at $\lambda = 22.5^{\circ}$ then becoming positive for incidences greater than 16.5°.

5.3 Differences resulting from the addition of the nose probe and lug

Fig.24 shows that the addition of the nose probe and launching lug to the model, to make it fully representative of the flight condition, has a large influence on the rolling moments acting at the higher incidences. The lateral loading on the model is also affected at some attitudes (Fig.19 and 20) due to these configuration changes, but the normal force and pitching moment is almost unaltered (Figs.17 and 18). It can also be seen by comparing the results for the pointed nose with those for the model with the nose probe alone and the nose probe with the lug, (Fig.24), that the large changes in rolling moment that occur are a consequence of adding the nose probe, the addition of the lug having only a minor influence. This large effect of the nose probe is also demonstrated by measurements made on the model with the nose probe rotated about the body centre line, through 180° (to achieve this condition the first two inches of the body also had to be rotated). Comparing these results (Fig.24) with those obtained with the nose probe in the original position shows that the incremental changes in rolling moment associated with the nose probe are of opposite sense for the configuration with the nose probe rotated through 180°.

Figs.25, 26 and 27 show the variation of rolling moment with roll angle for the model configurations with the nose probe in position. Comparing these figures with Fig.15 show that the approximately regular sinusoidal variation of rolling moment with roll angle that occurred with the pointed nose is drastically altered by the nose probe.

Flow pictures taken at a model attitude $\sigma = 20^{\circ}$ $\lambda = 0^{\circ}$ for both the pointed and nose with probe configurations (Fig.28) show that although the probe causes no obvious flow asymmetries over the nose portion of the model, at the fins there is a definite asymmetry in the flow. This is indicated by the differences in the flow patterns on the body between the upper fin and the port and starboard fins (Fig.28a). The lack of symmetry in the flow at the rear of the model is also illustrated by the flow patterns on the support sting, with the nose probe in position the flow on the sting at the base of the model is strongly biased to the starboard side.

An inspection of the spherical nose of the probe made after the tests revealed that it was not quite geometrically perfect. The error was such that the nose of the probe was 0.08 mm off the centre line of the cylindrical portion of the probe in the direction shown in Fig.2b. This small manufacturing error is most probably a contributory cause of the large rolling moments associated with the probe, the distortion giving rise to a markedly asymmetric body - vortex system. It is thought, however, that a spherical nose even if geometrically perfect, is more prone to give rise to an asymmetric body vortex system than a pointed nose because the point of the latter acts a definite trigger for the start of the body vortices.

6 CONCLUSIONS

The results of the tests made on the bomb model M557A at $M = 0.50$ indicate that the discrepancy between the rolling moments measured in the A.R.A. wind tunnel tests and the values derived from the free flight tests cannot be directly attributed to scale-effect. The variation of rolling moment coefficient with incidence measured in the present tests for the model with pointed nose shows little dependence on Reynolds number, for a range $R = 1.29 \times 10^6$ to 2.60×10^6 and these results largely confirm the A.R.A. results.

The addition of the nose probe and launching lug to the model causes large changes in the character of the induced rolling moments at high incidence. These changes in rolling moment are mainly associated with the nose probe, although the launching lug caused measurable differences. With the nose probe in position large rolling moments act on the model at symmetric attitudes and this can be attributable in part to a slight asymmetry of the nose of the probe. This dependence of the rolling moment on the geometric accuracy of the nose of the probe is therefore likely to make it extremely difficult in practice to obtain a good correlation of rolling moment results between different tests on configurations of this type, although particular attention to symmetry will minimize the discrepencies.

Table 1

TEST RANGES, FIRST SERIES OF TESTS

MODEL CONFIGURATION, ORIGINAL POINTED NOSE

Reynolds number (based on body dia.)	Incidence angle setting σ^{o}	Roll angle setting λ^{o}
1.29×10^{6}	-2 to 20	0, ±22.5, ±45, ±67.5, ±90, +112.5 135, 157.5, 180, 202.5, 225, 247.5, 270
	12, 14, 16, 18, 20	-90 to 270
1.92×10^{6}	-2 to 20	0, 22.5, 45, 67.5, 90
2.60×10^{6}	-2 to 20	0, 22.5, 45, 67.5, 90

Table 2

TEST RANGES, SECOND SERIES OF TESTS

REYNOLDS NUMBER (BASED ON BODY DIA.) 1.29×10^{6}

Model configuration	Incidence angle setting σ^{o}	Roll angle setting λ^{o}
Replacement pointed nose	-2 to 20	0, 22.5, 45, 67.5
Nose probe + lug	-2 to 20	0, 22.5, 45, 67.5, 180, 225
	10, 14, 16, 18, 20	-90 to 270
Nose probe	-2 to 20	0, 22.5, 45, 67.5, 180, 225
	10, 14, 16, 18, 20	-90 to 270
Nose probe rotated 180^{o}	-2 to 20	0, 22.5, 45
	10, 14, 16, 18, 20	-90 to 90

SYMBOLS

b	maximum body diameter.
q	tunnel dynamic head $(\frac{1}{2}\rho V^2)$
S	maximum body cross sectional area
C_z'	normal force coefficient (in the total incidence plane) $\frac{Z'}{qS}$
C_m'	pitching moment coefficient (in the total incidence plane) $\frac{m'}{qSb}$
C_y'	sideforce coefficient (normal to the total incidence plane) $\frac{Y'}{qS}$
C_n'	yawing moment coefficient (normal to the total incidence plane) $\frac{n'}{qSb}$
C_l	rolling moment coefficient $\frac{l}{qSb}$
λ	incidence plane angle (sting roll angle)
σ	total incidence (sting pitch angle)
R	Reynolds number based on model diameter

REFERENCES

No.	Author(s)	Title, etc.
1	C.W. Rhodes J.H.W. Shannon	Results and conclusions of the joint R.A.E./W.R.E. research programme on the flight dynamics and ballistic consistency of freely falling missiles Part 1 *Bombs stabilised by fixed cruciform fins.* R.A.E. Technical Report 65200, ARC 28322, WRE HSA 20 (1965)
2	J.D. Nicolaides	A review of some recent progress in the understanding of catastrophic yaw. AGARD Report 551 (1966)

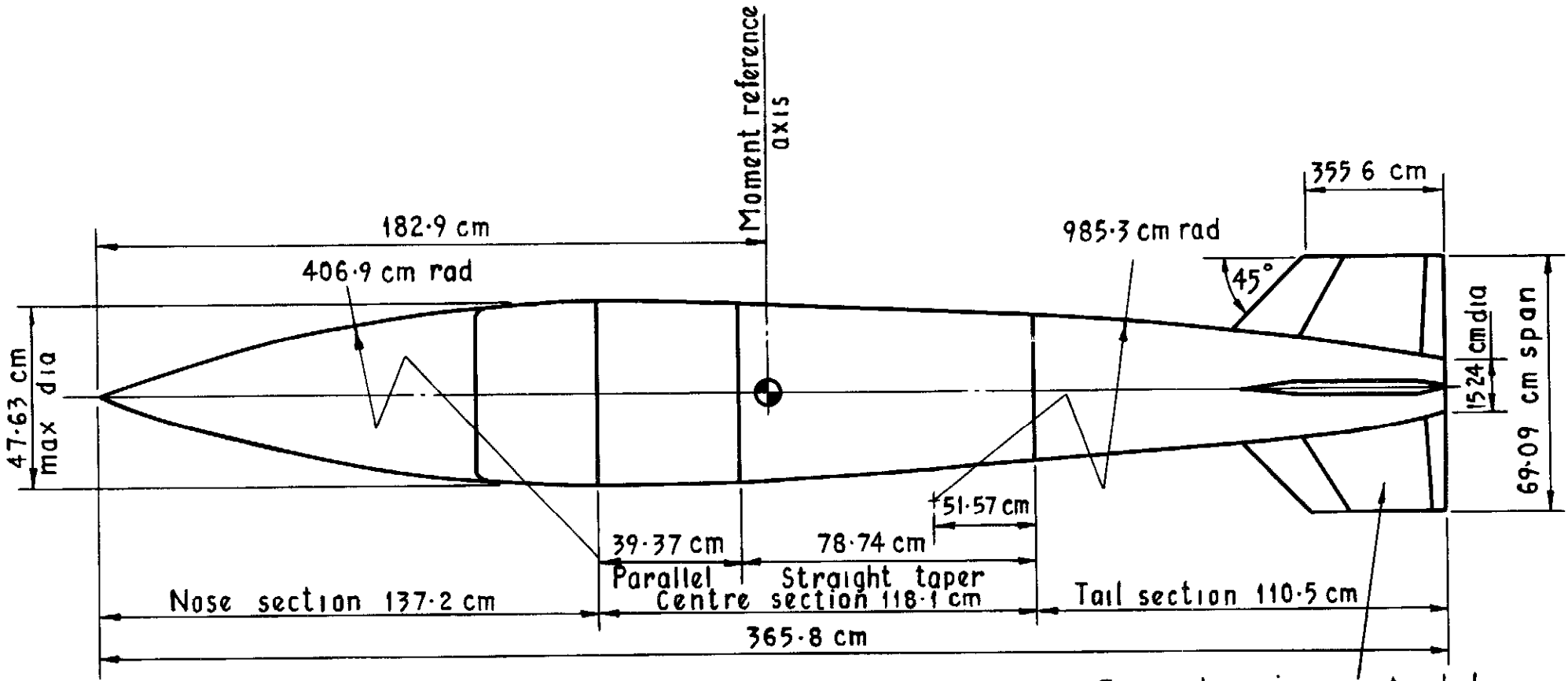

Fig. 1 Geometric details of M557^{A} bomb

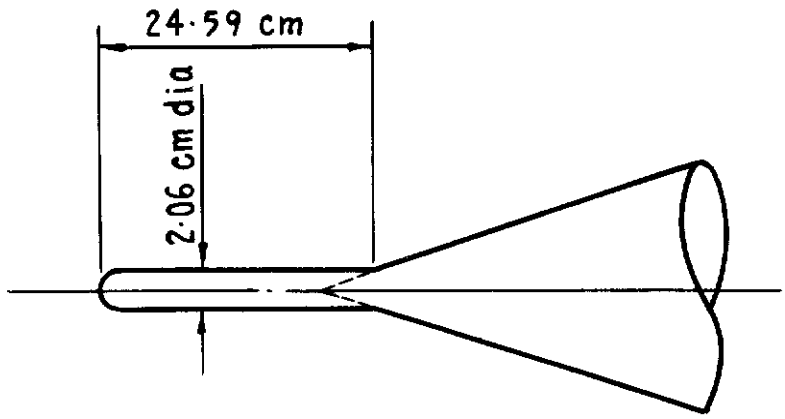

a Nose probe

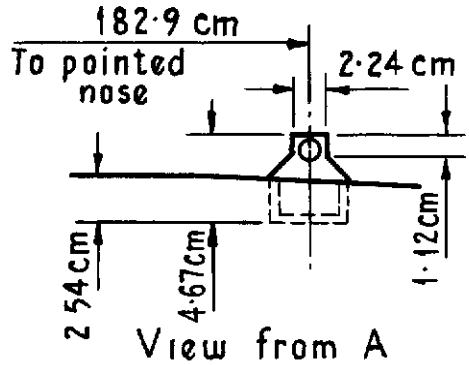

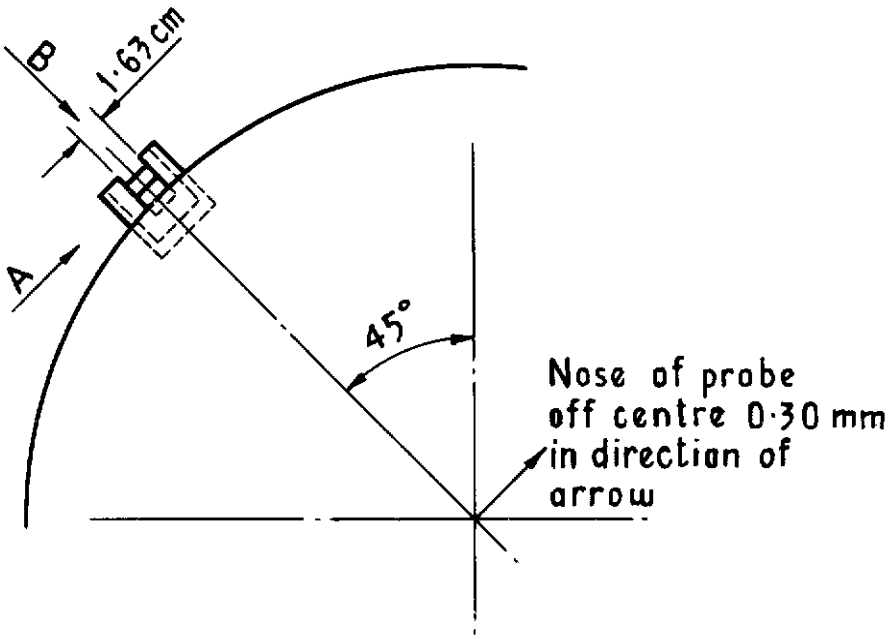

View from rear of bomb at $\lambda = 0°$ (fins vertical and horizontal)

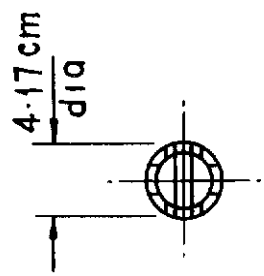

View from B

b Launching lug

All dimensions refer to full scale bomb
Model scale : ¼ full scale

Fig. 2a&b Geometric details of the M557^{A} bomb nose probe and lug

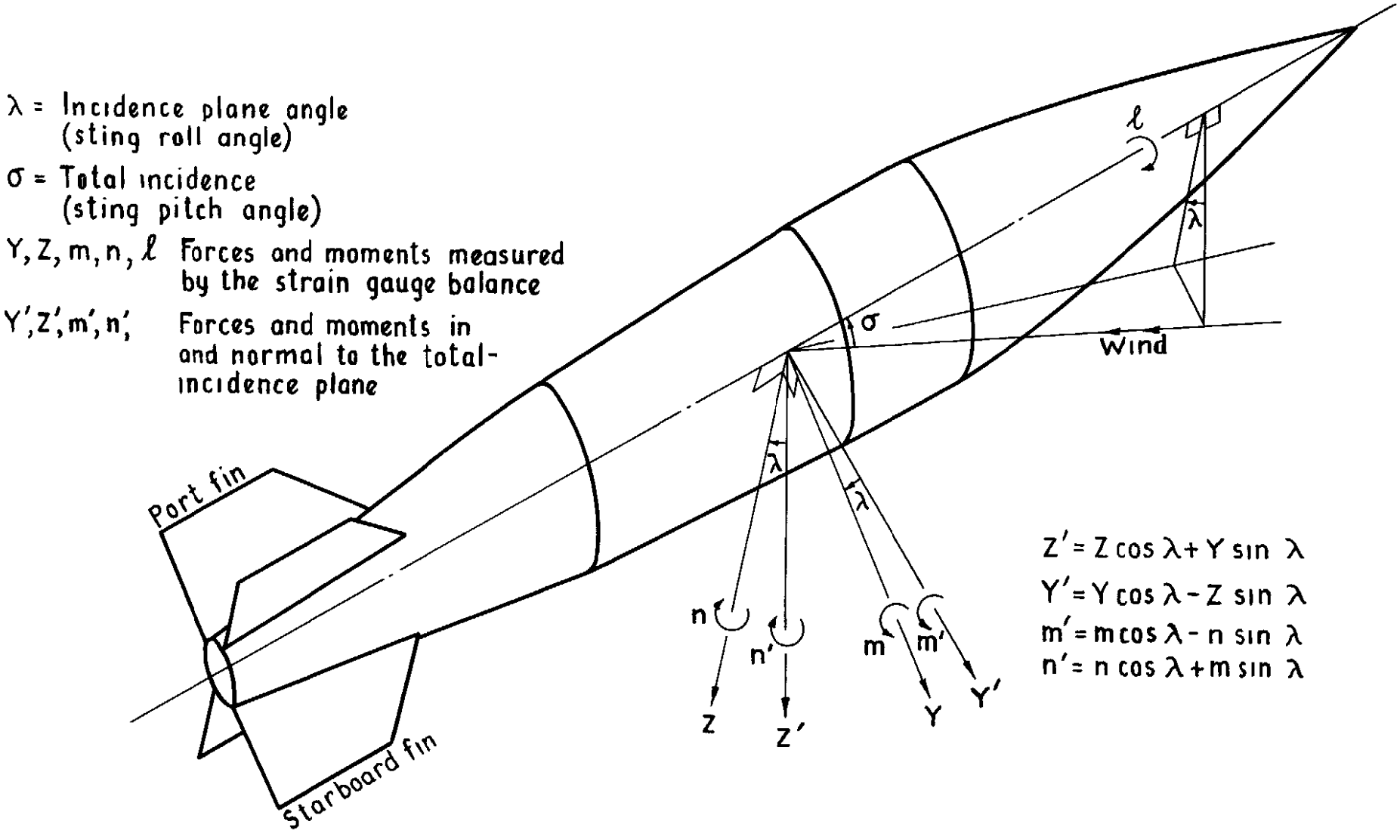

Fig 3 System of axes

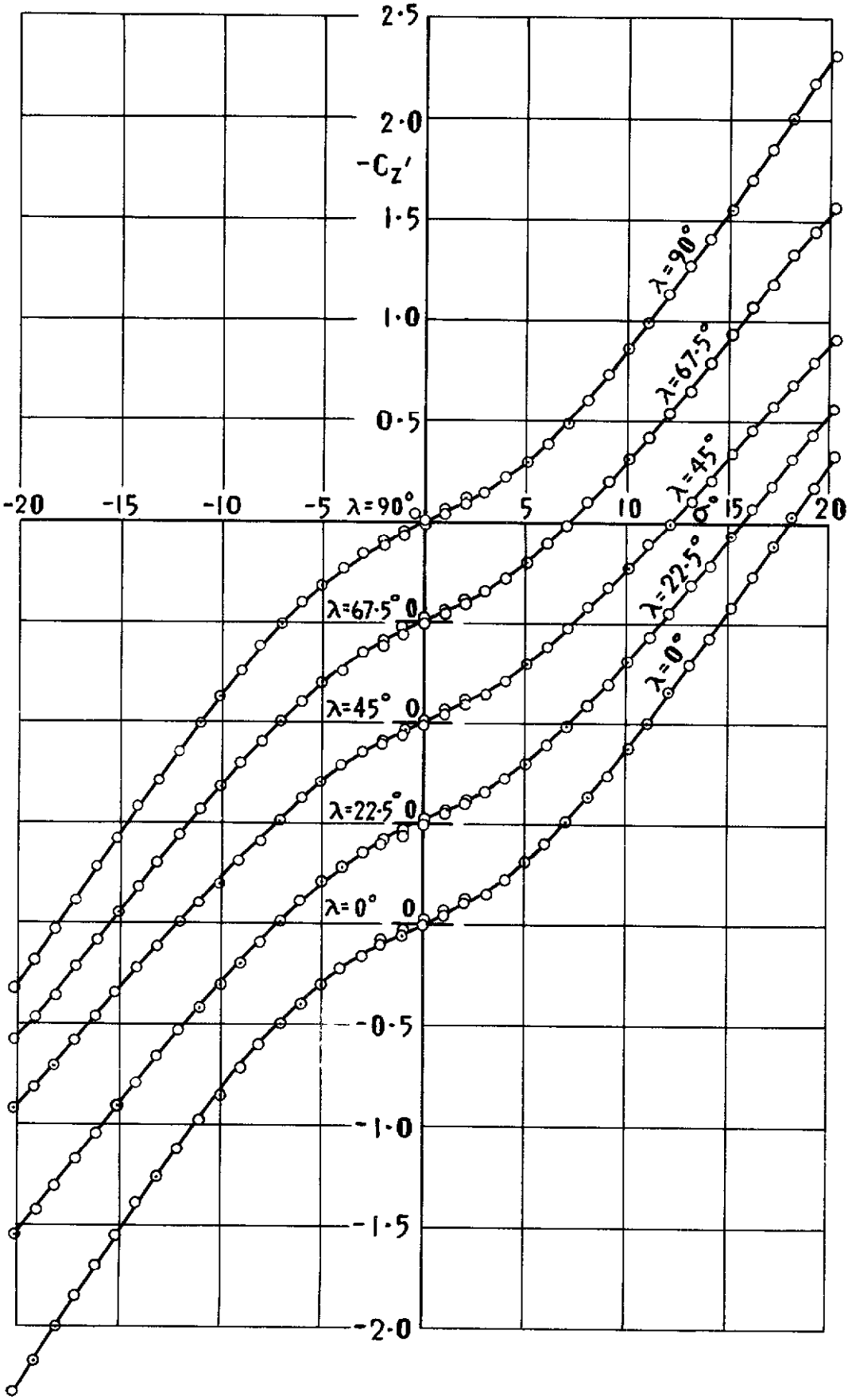

Fig 4a $C_{z'}$ vs σ, at constant λ, M=0·50, $R = 1{\cdot}29 \times 10^6$

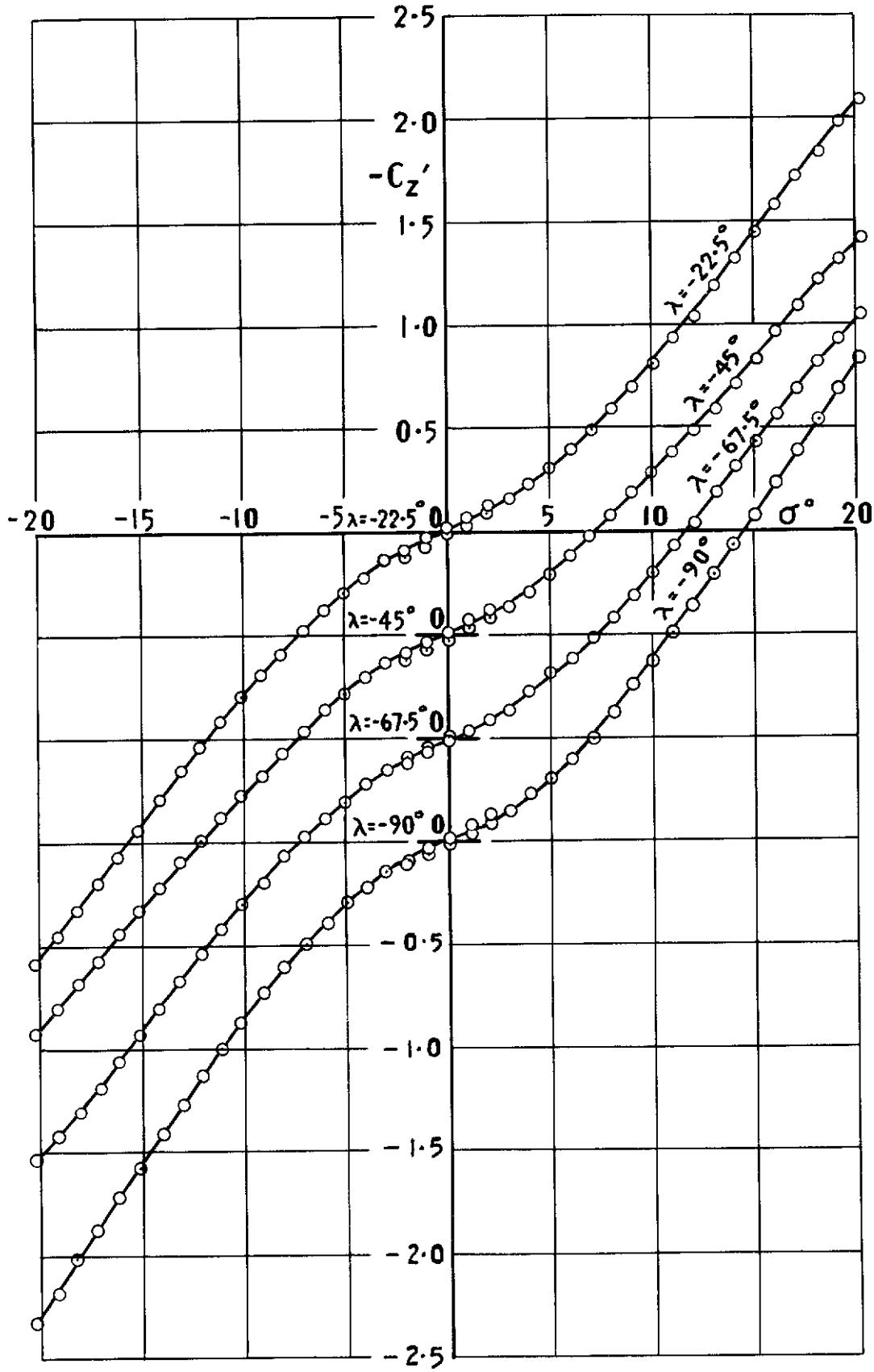

Fig 4b C_Z' vs σ, at constant λ, M=0·50, R = 1·29 x 10^6

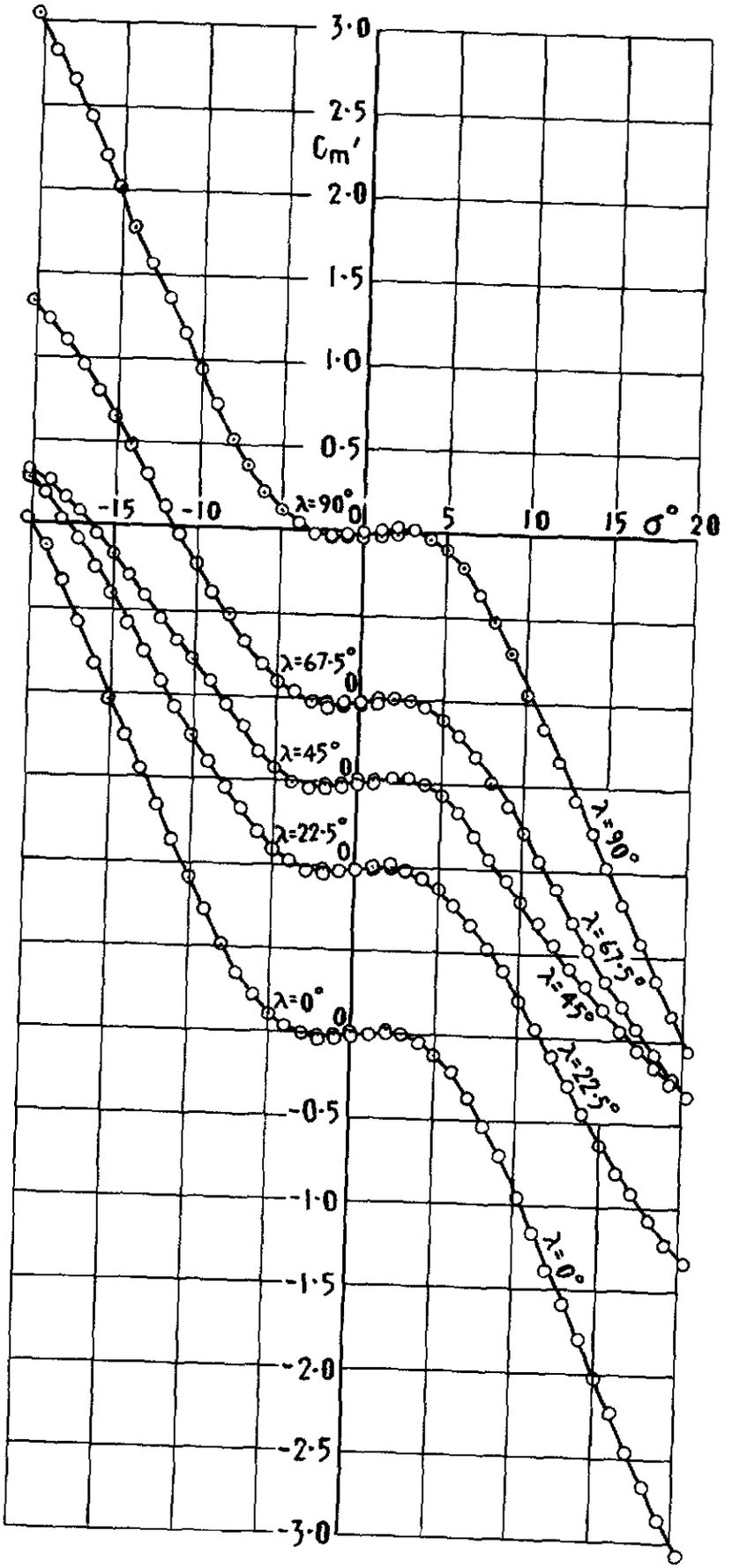

Fig 5a Cm' vs σ, at constant λ, M=0·50, R = 1·29 x 10^6

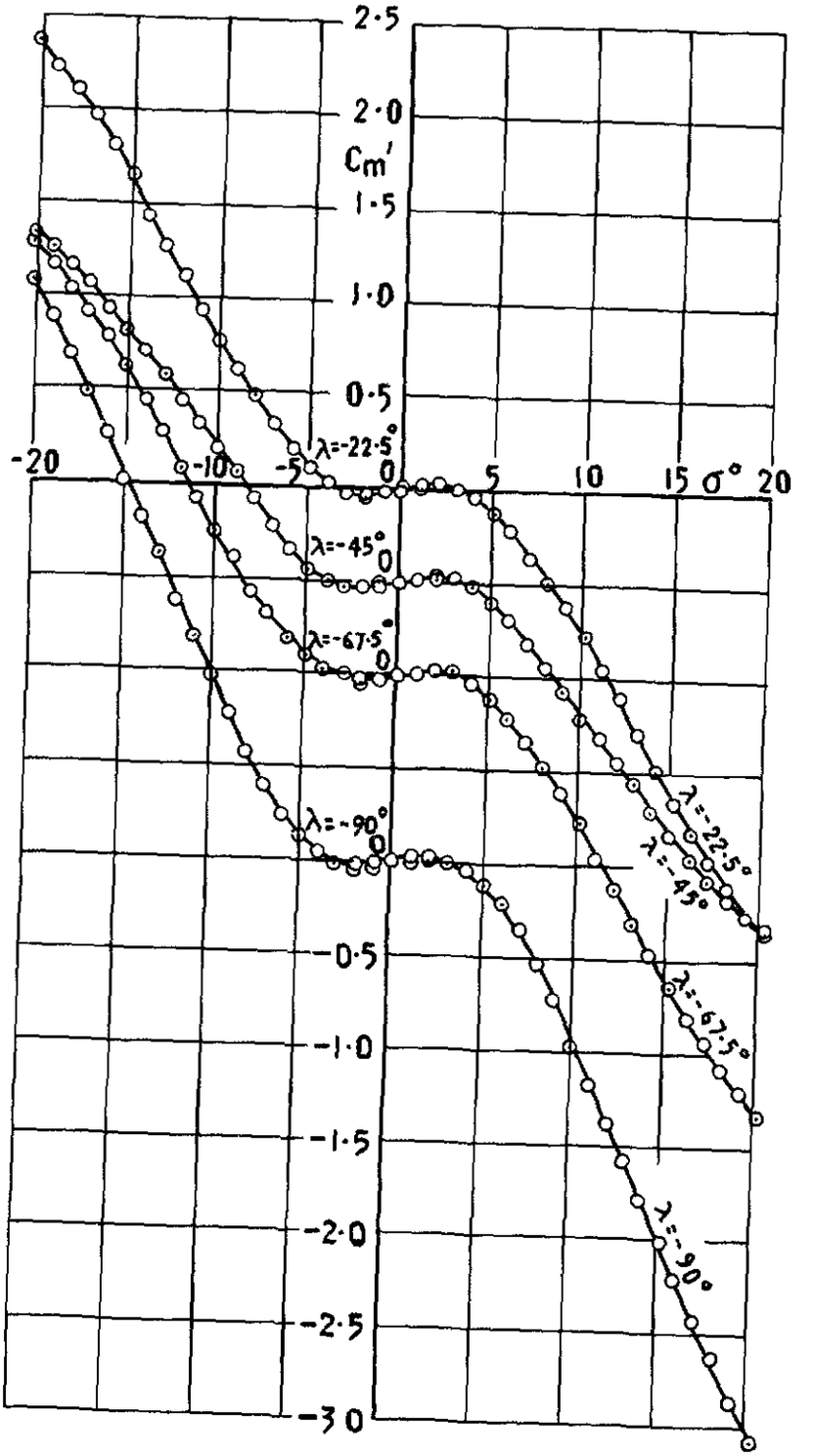

Fig. 5b C_m' vs σ, at constant λ, M=0·50, R = 1·29 x 10^6

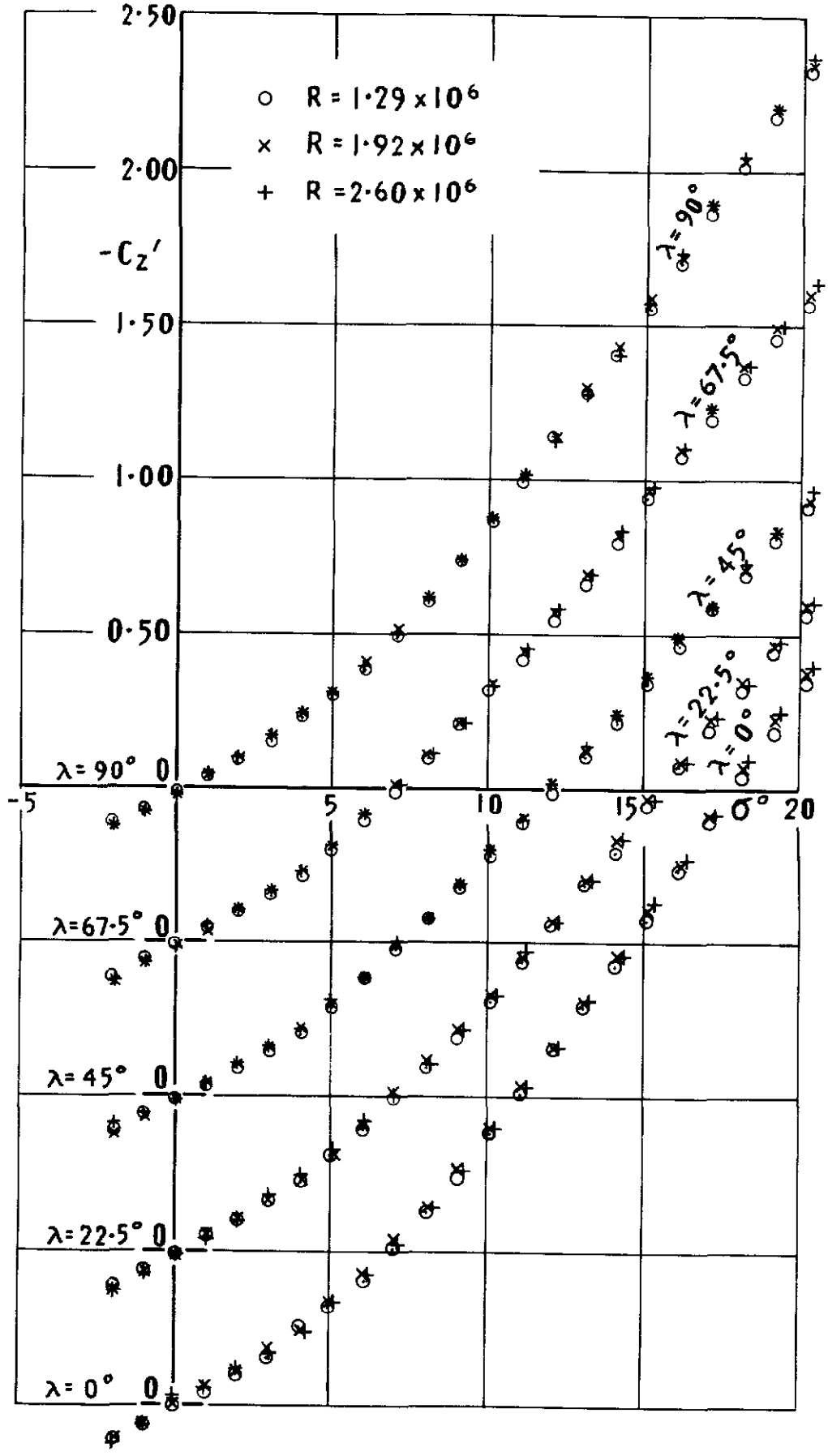

Fig.6 Comparison of C_z' vs σ at $M = 0{\cdot}50$ for Reynolds numbers $1{\cdot}29 \times 10^6$, $1{\cdot}92 \times 10^6$ and $2{\cdot}60 \times 10^6$

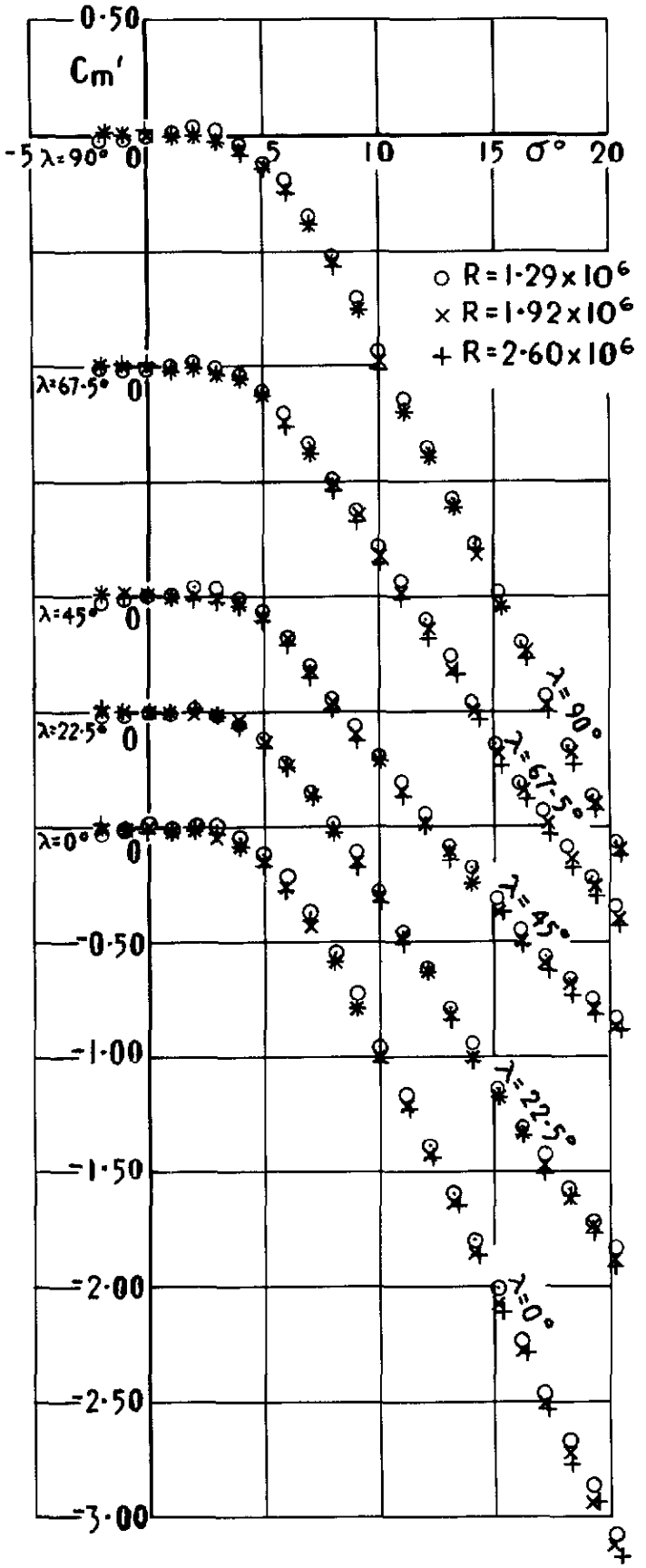

Fig.7 Comparison of $C_{m'}$ vs σ at $M=0{\cdot}50$ for Reynolds numbers $1{\cdot}29\times10^6$, $1{\cdot}92\times10^6$ and $2{\cdot}60\times10^6$

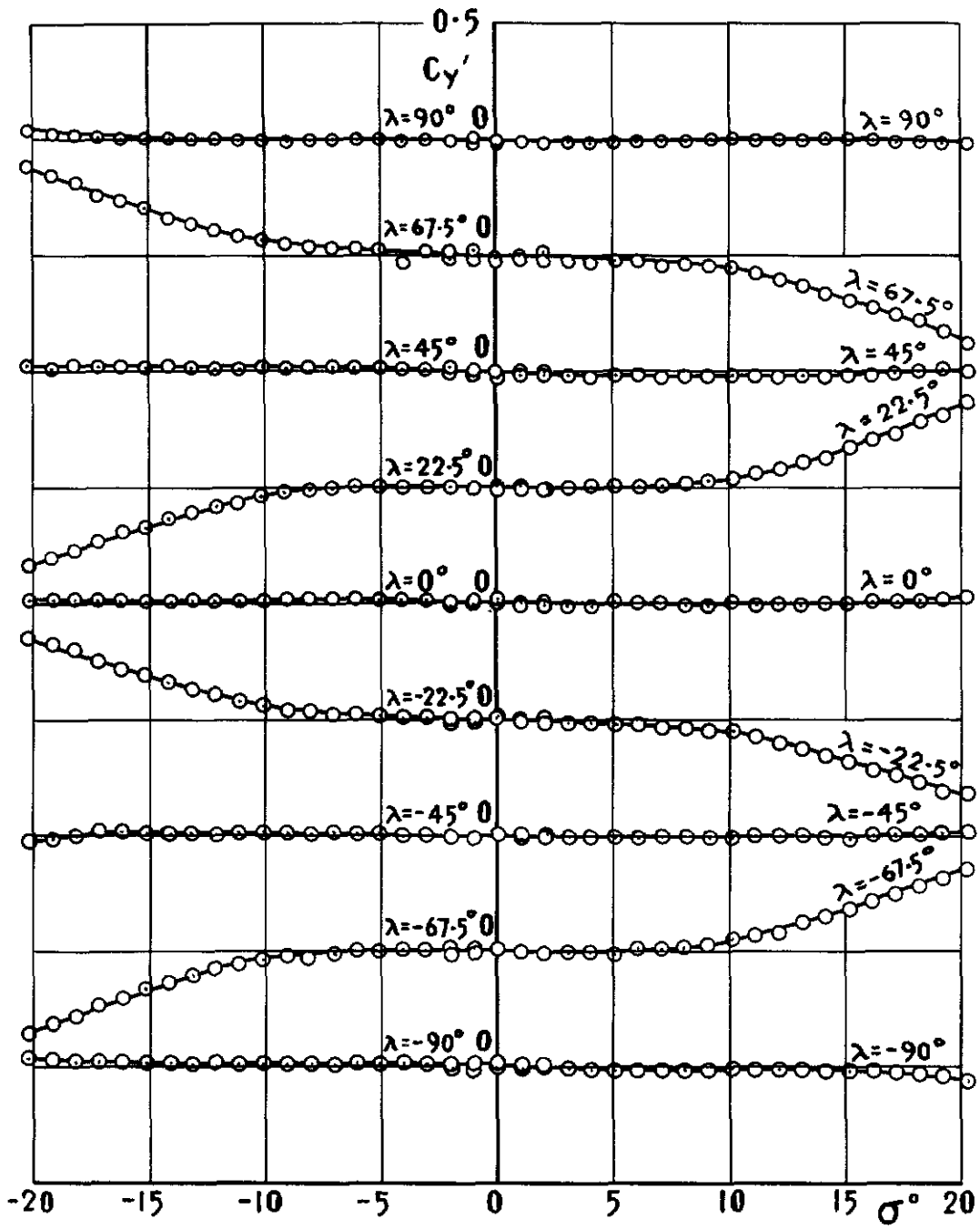

Fig. 8 $C_{y'}$ vs σ, at constant λ, M=0·50, $R = 1 \cdot 29 \times 10^6$

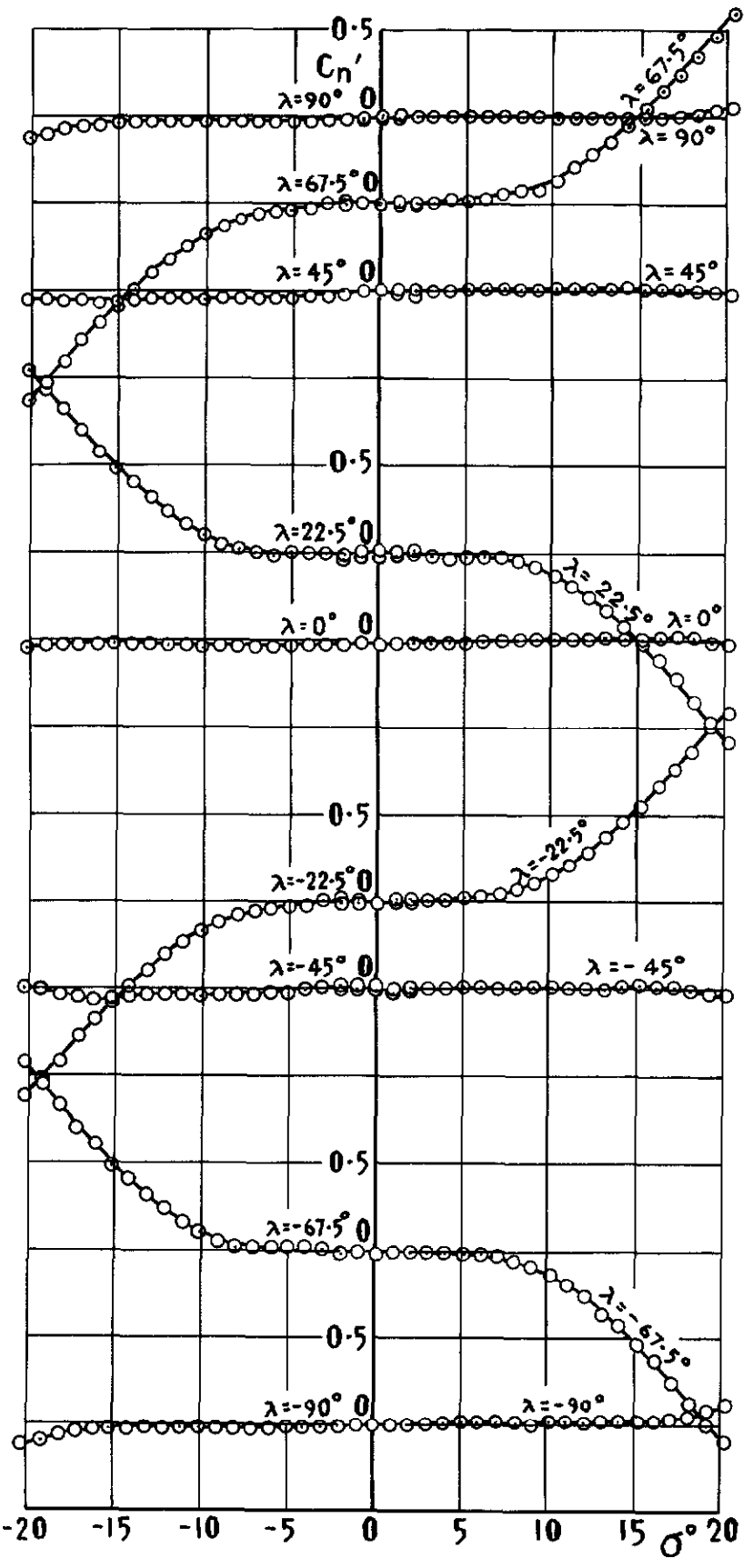

Fig. 9 C_n' vs σ, at constant λ, M=0 50, $R = 1 \cdot 29 \times 10^6$

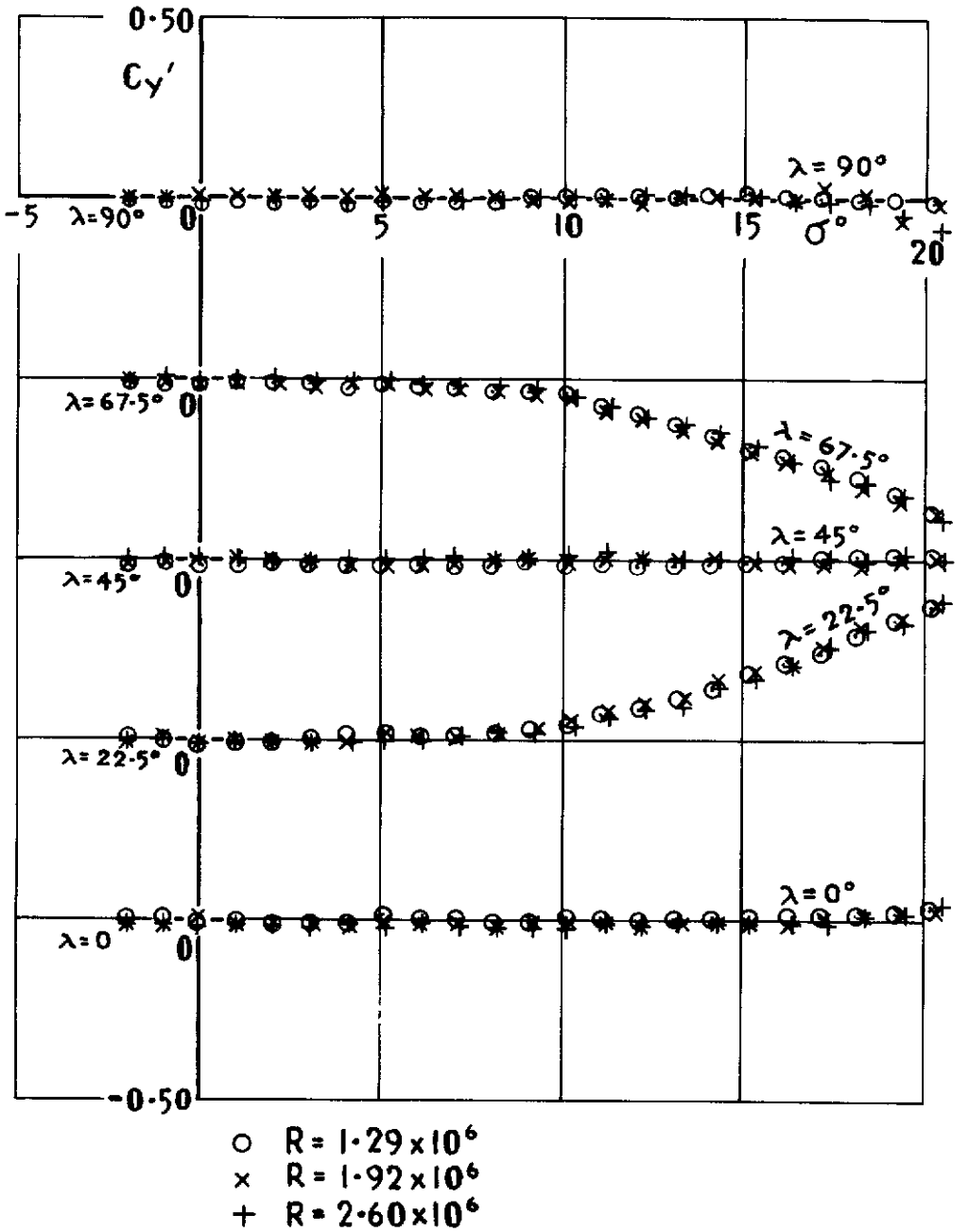

Fig.10 Comparison of Cy' vs σ at M = 0·50
for Reynolds numbers $1{\cdot}29 \times 10^6$, $1{\cdot}92 \times 10^6$ and $2{\cdot}60 \times 10^6$

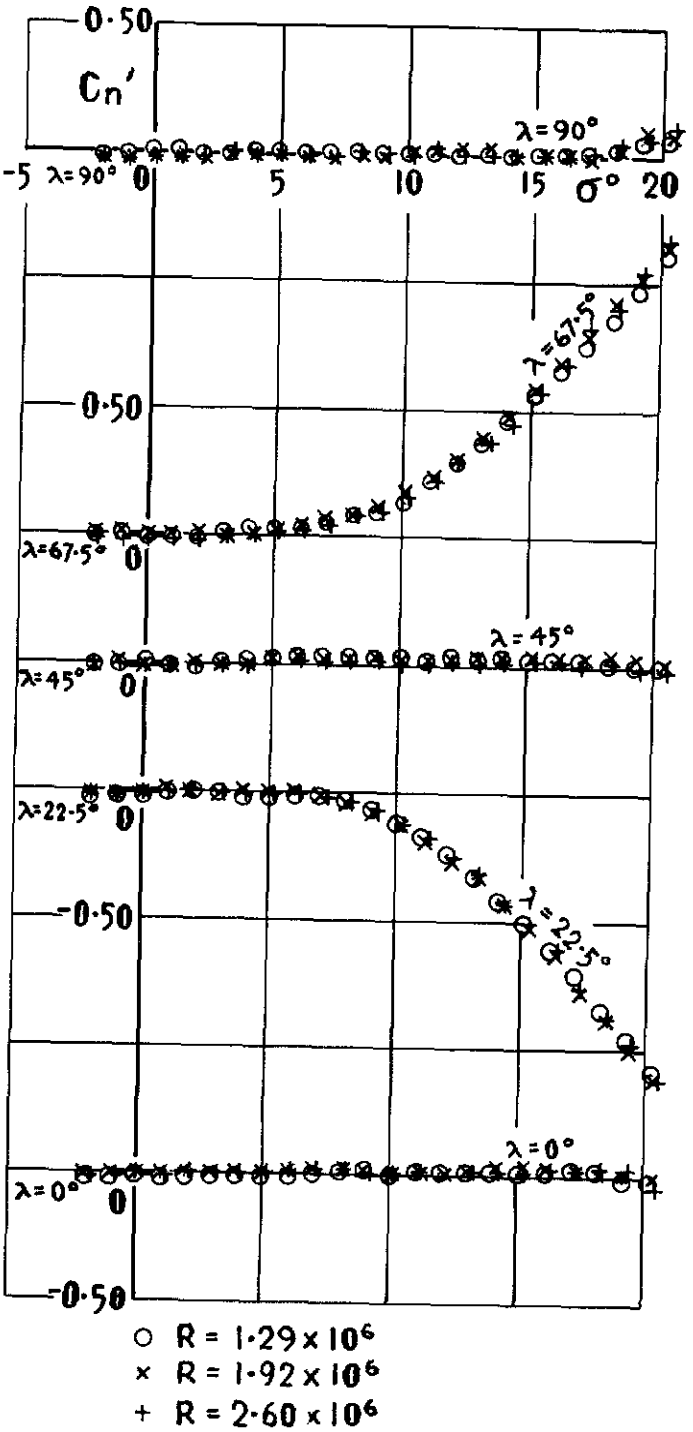

Fig.11 Comparison of $C_{n'}$ vs σ at $M = 0 \cdot 50$ for Reynolds numbers $1 \cdot 29 \times 10^6$, $1 \cdot 92 \times 10^6$ and $2 \cdot 60 \times 10^6$

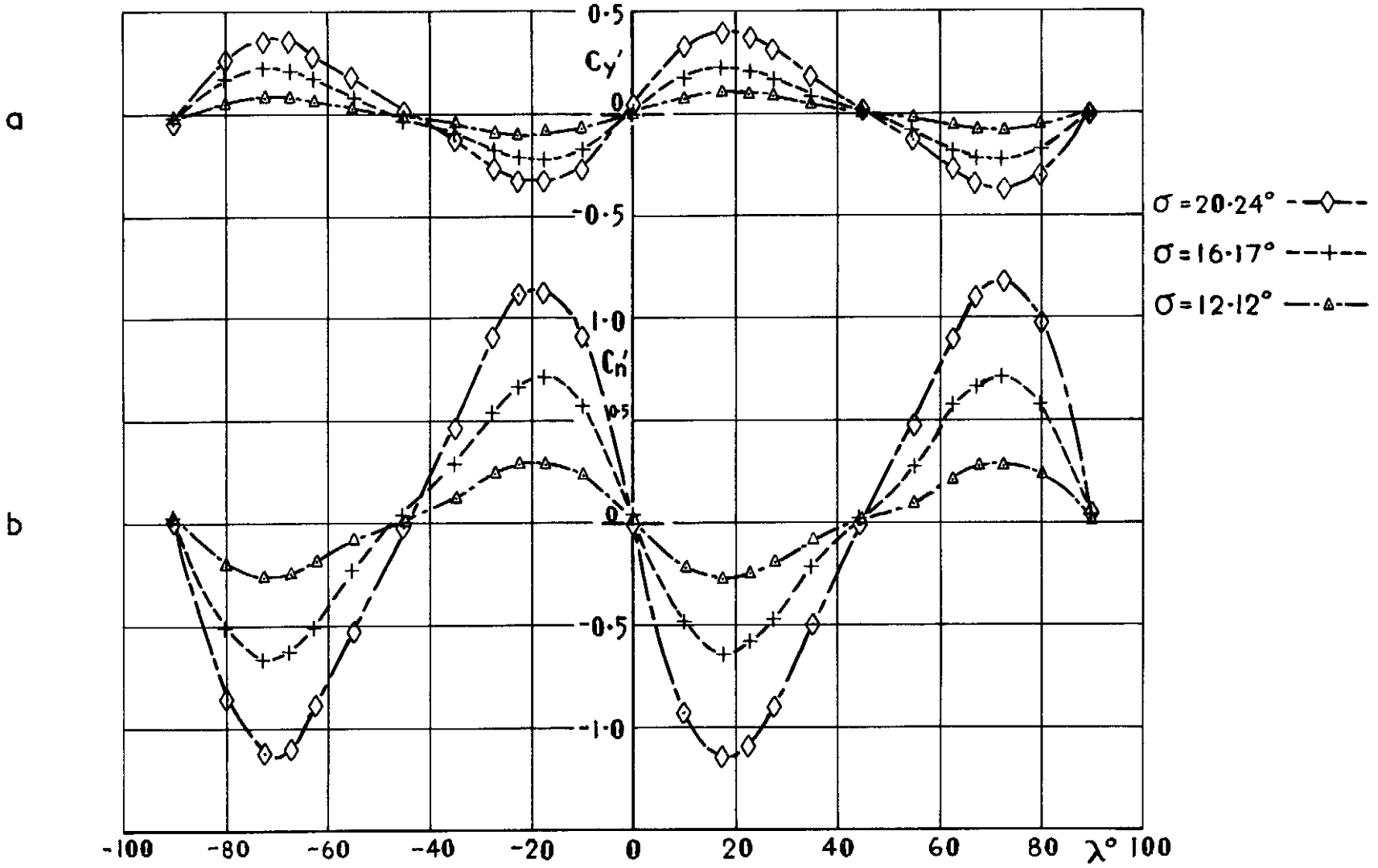

Fig. 12a & b C_y' and C_n' vs λ, at constant σ, $\lambda = -90°$ to $+90°$
$M = 0·50$, $R = 1\,29 \times 10^6$

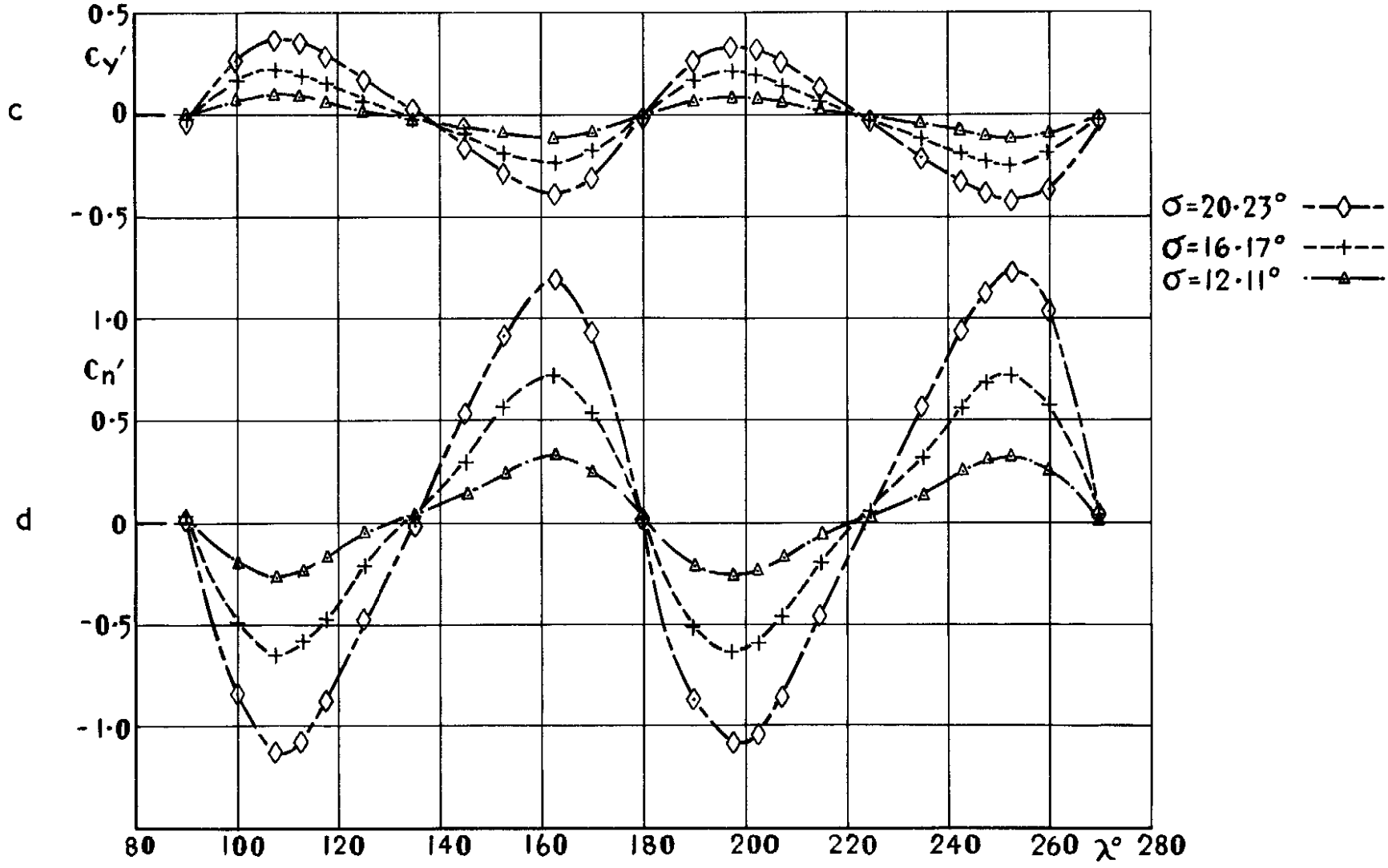

Fig.12c&d $C_{y'}$ and $C_{n'}$ vs λ, at constant σ, λ = 90° to 270°
M = 0·50, R = 1·29 x 10^6

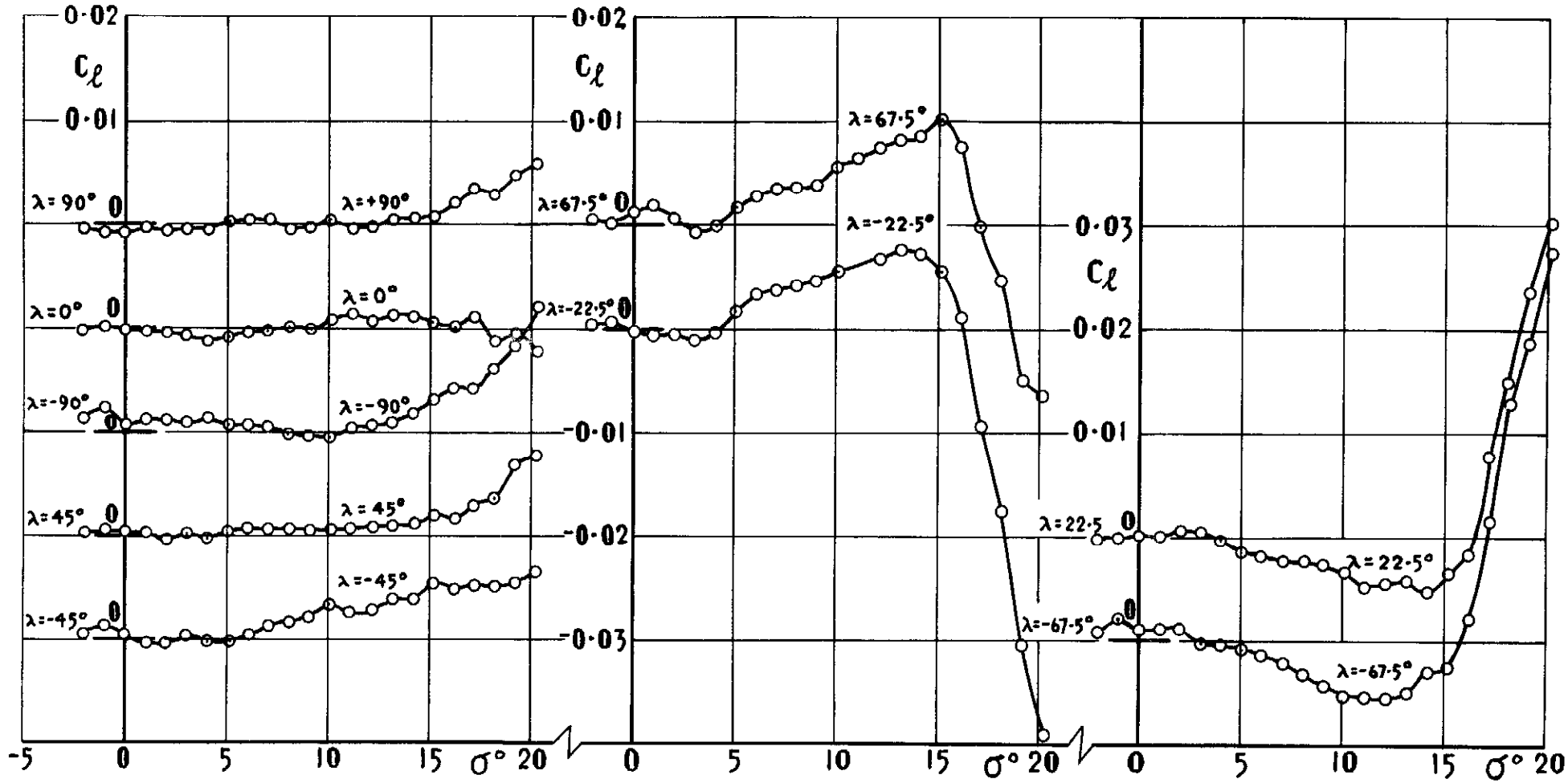

Fig 13a C_ℓ vs σ , at constant λ
M=0·50, R=1·29 x 10^6

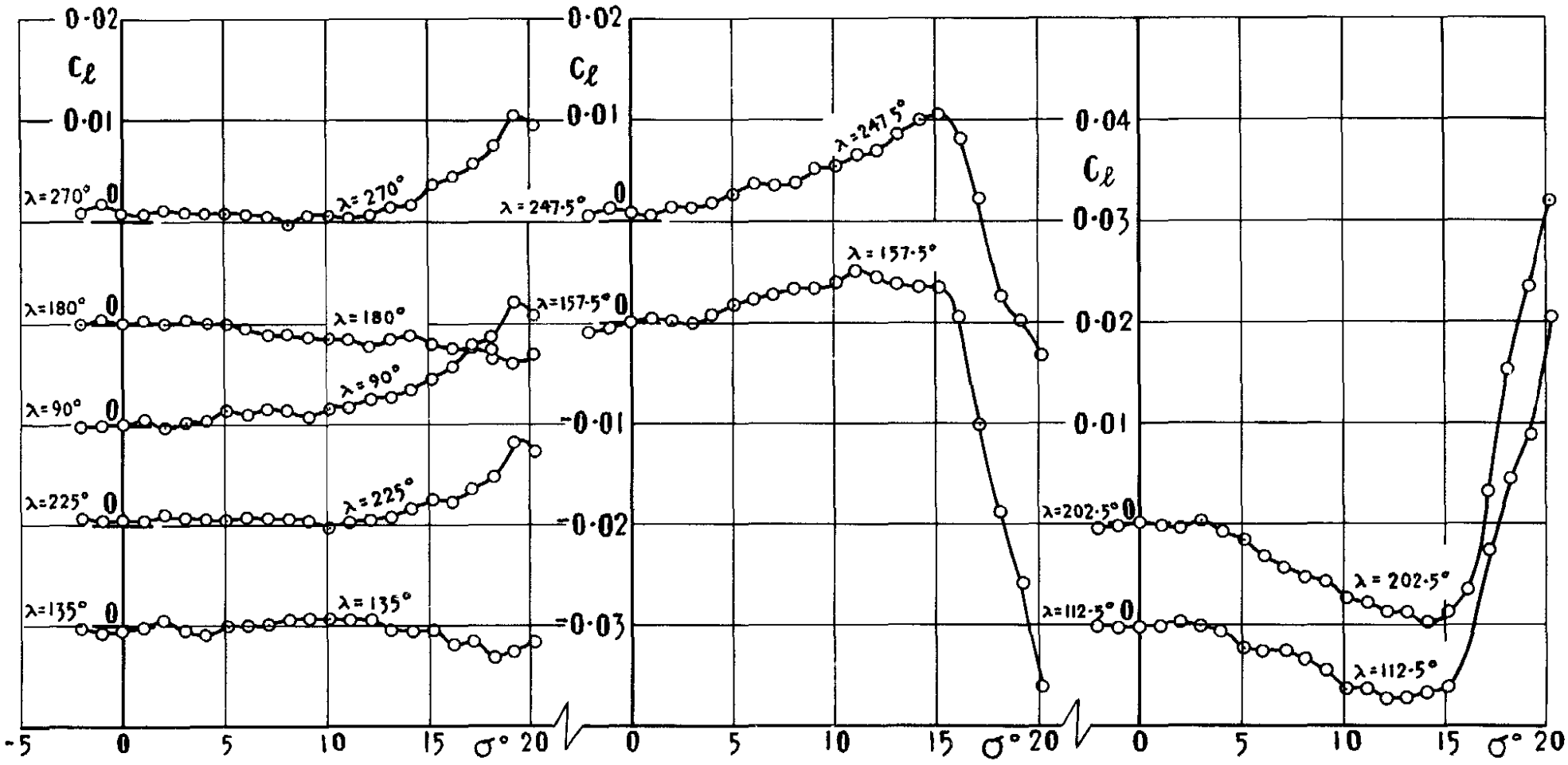

Fig. 13b C_ℓ vs σ, at constant λ
M = 0·50, R = 1·29 x 10^6

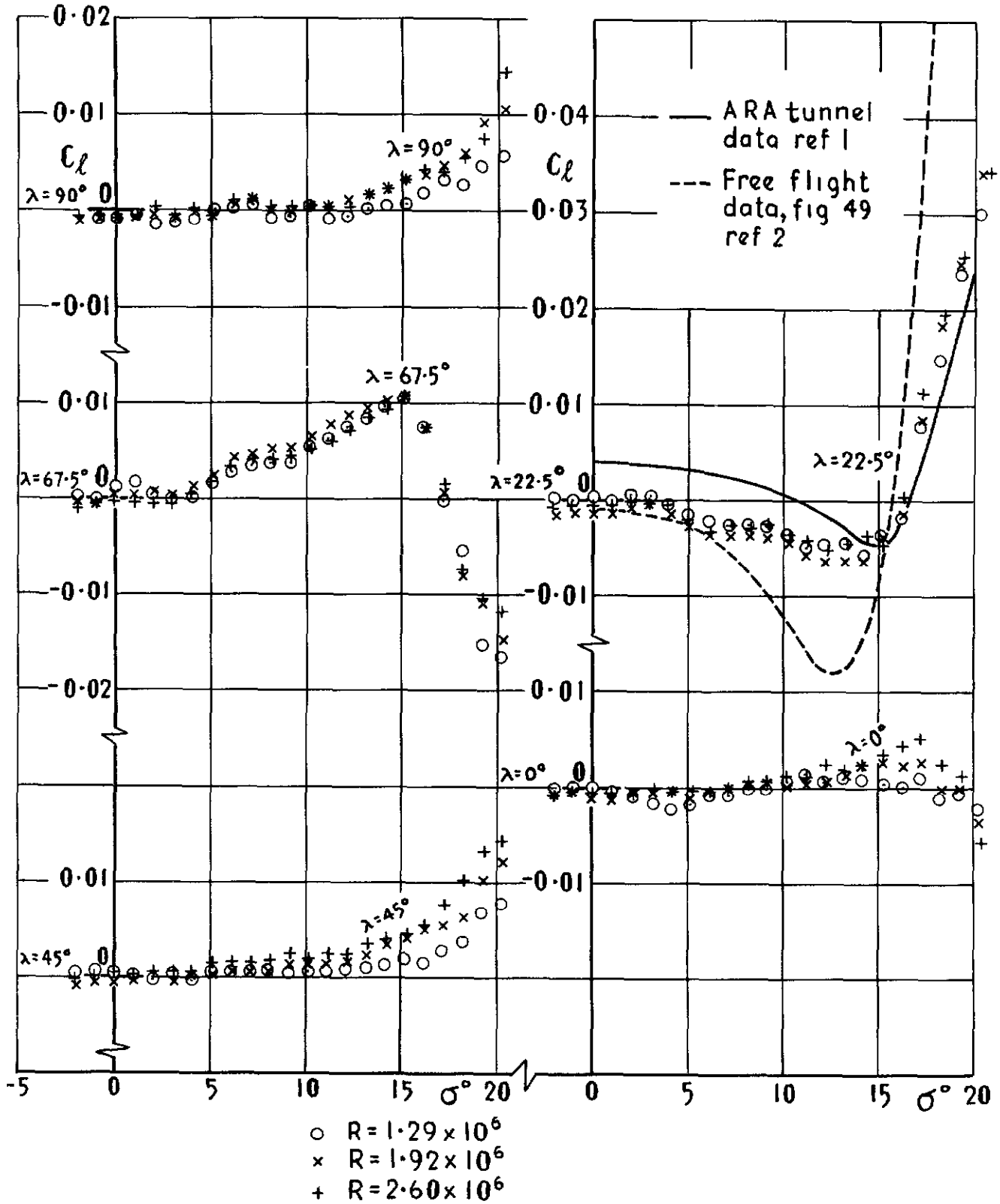

Fig.14 Comparison of C_ℓ vs σ at M = 0·50
for Reynolds numbers 1·29 x 10⁶, 1 92 x 10⁶ and 2·60 x 10⁶

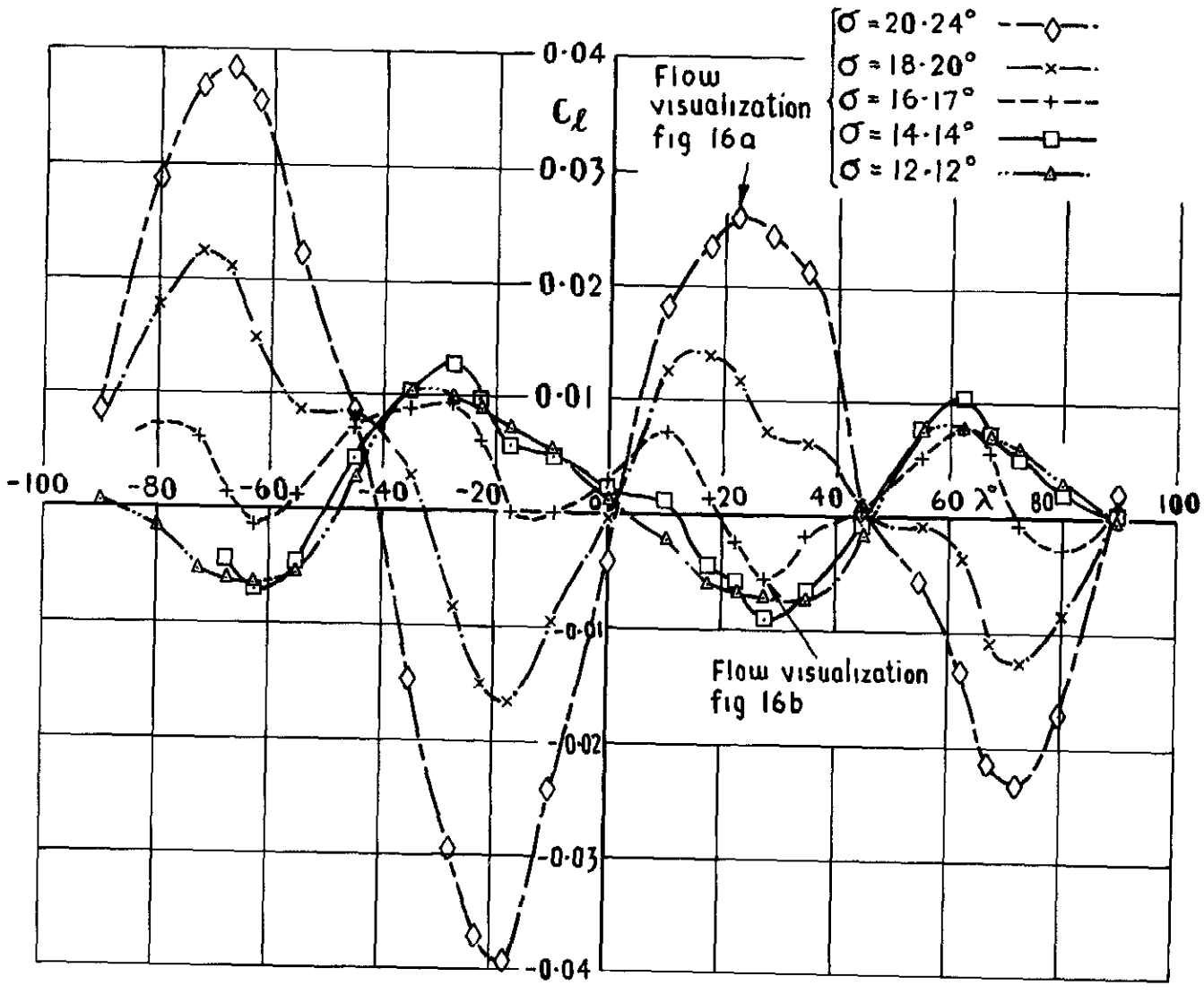

Fig 15a C_ℓ vs λ , at constant σ, $\lambda = -90^\circ$ to $+90^\circ$
M=0·50, R=1·29x10⁶

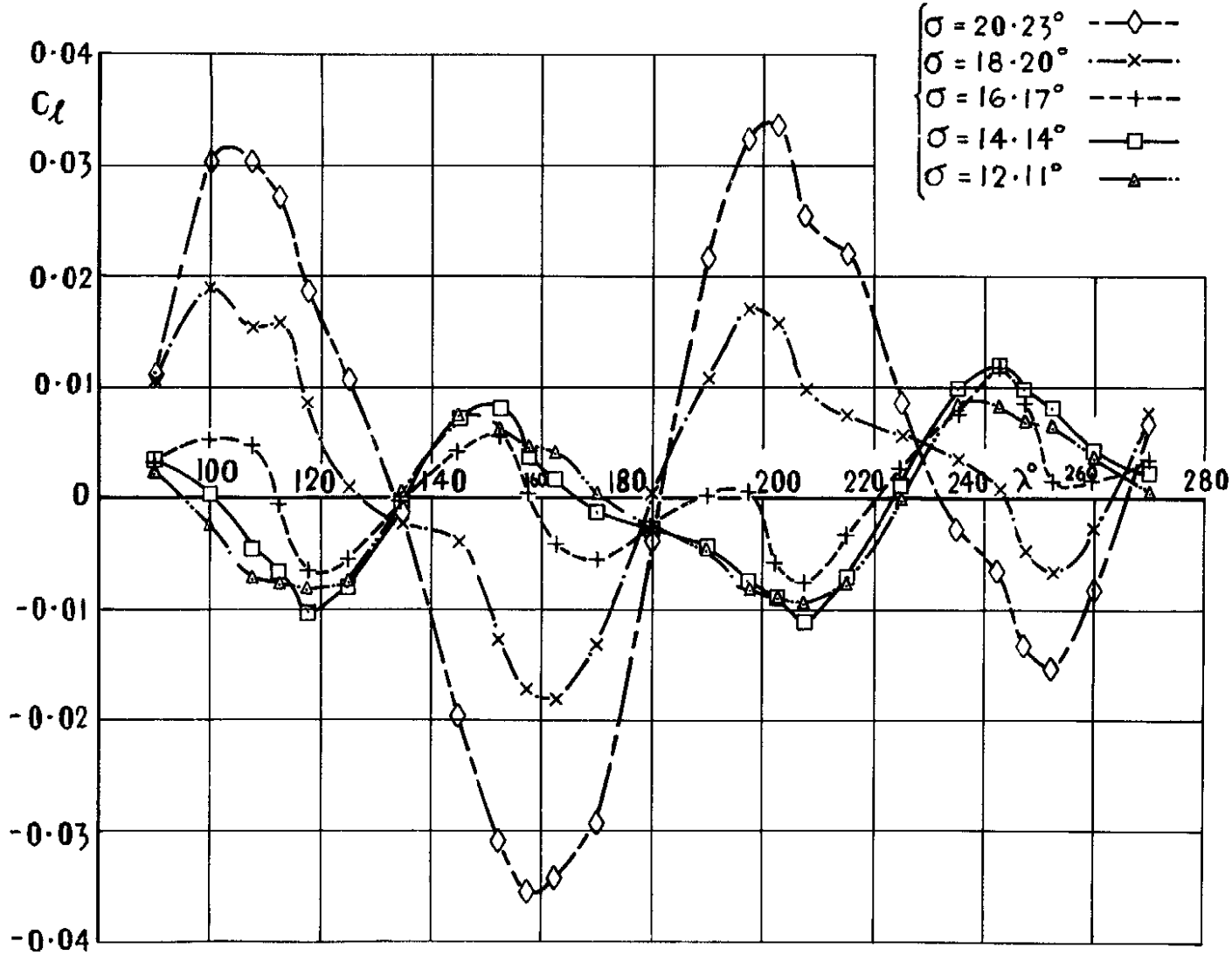

Fig 15b C_l vs λ , at constant σ , λ = 90° to 270°
M = 0 50, R = 1·29 x 10⁶

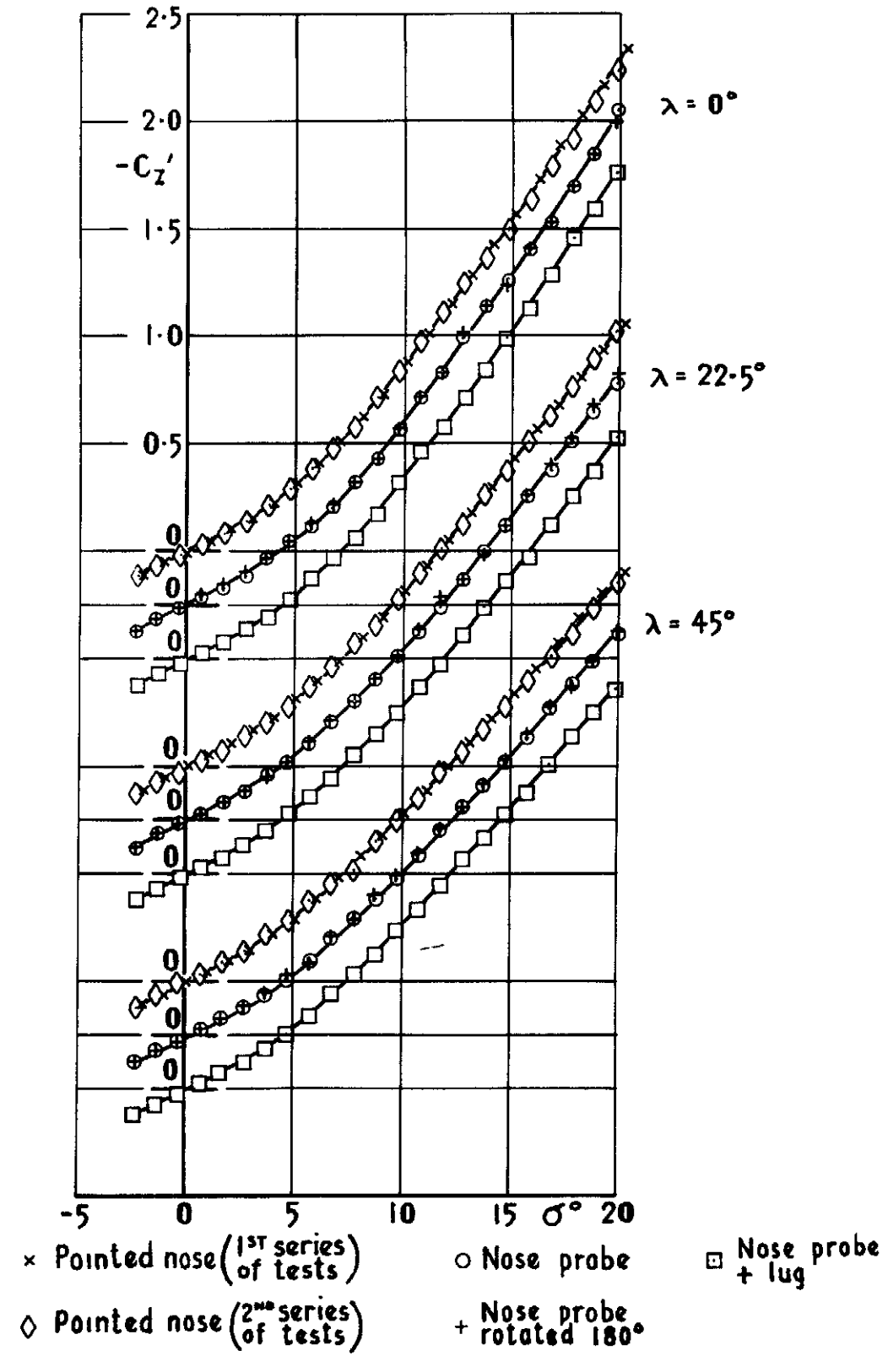

Fig.17a C_z' vs σ , M=0·50, R=1·29x10^6

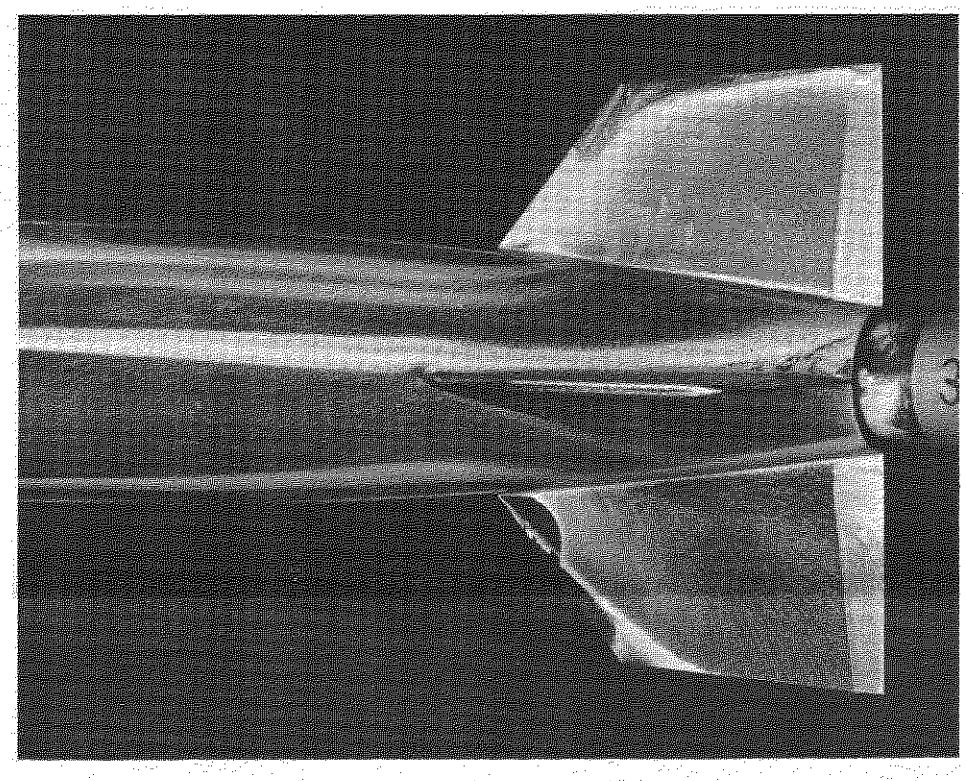

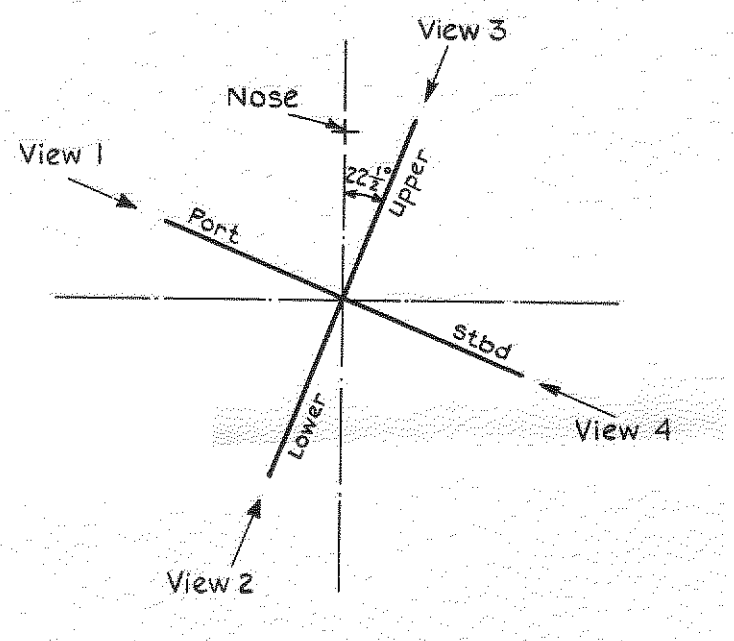

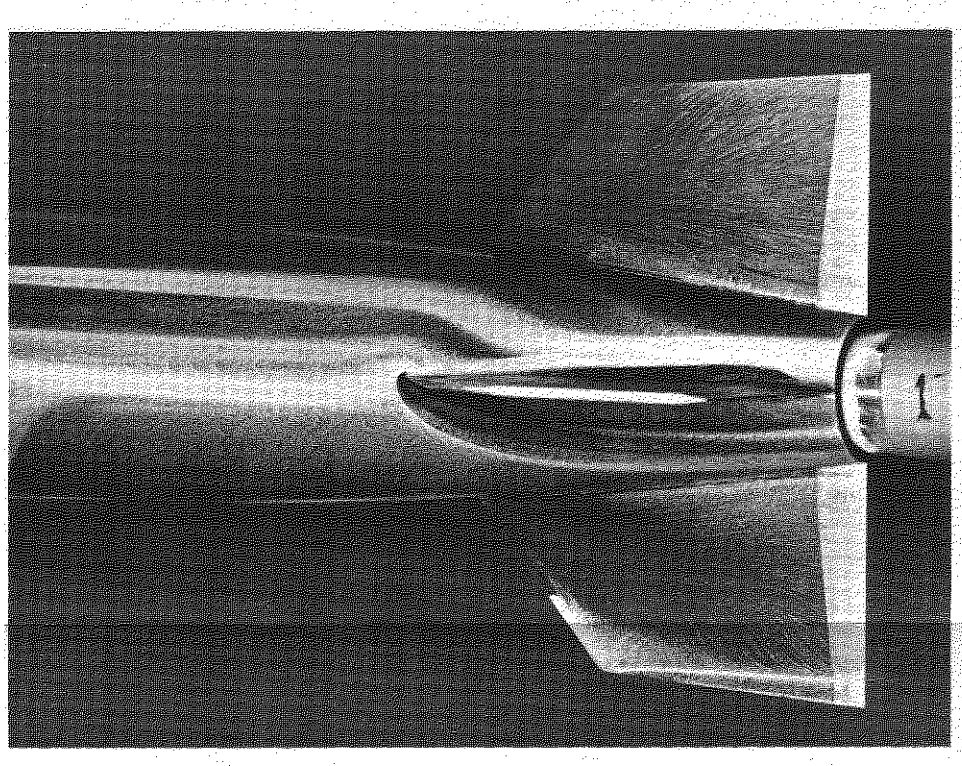

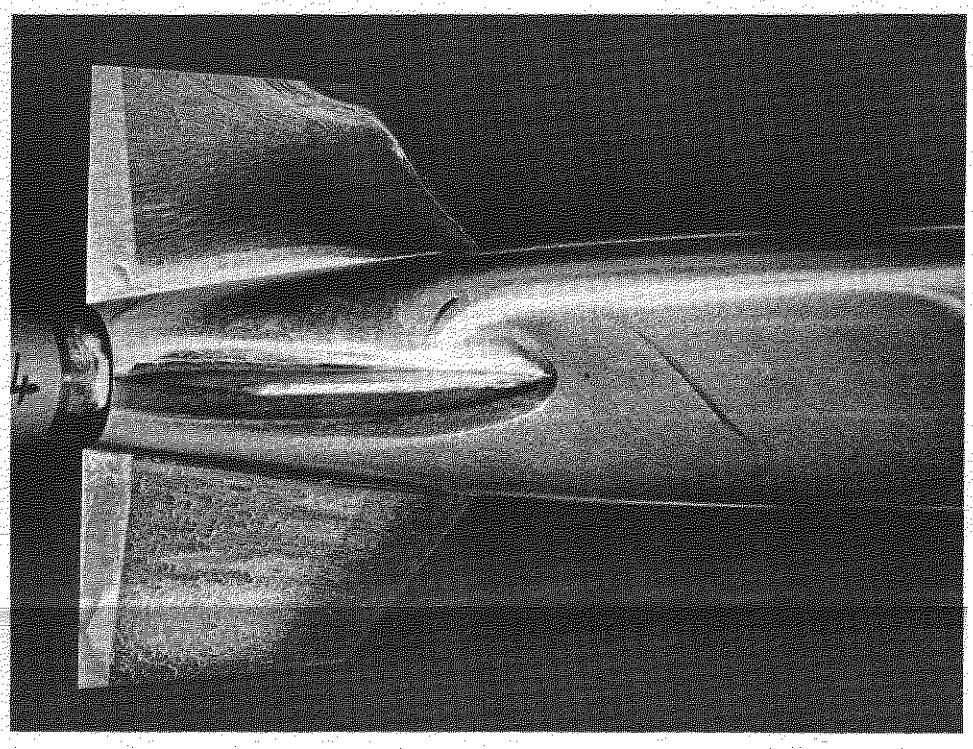

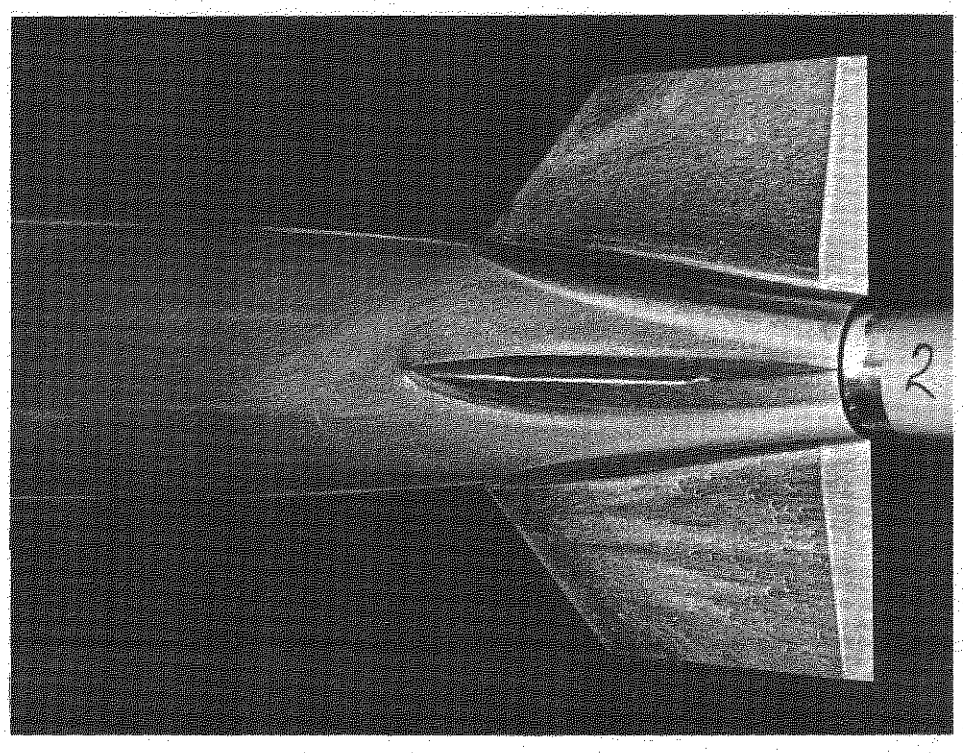

σ = 20.24° λ = 22.5° C_ℓ = 0.026

Fig.16a. Flow visualization.
Pointed nose (1st series of tests)
M=0.50 R=1.29 x 10^6

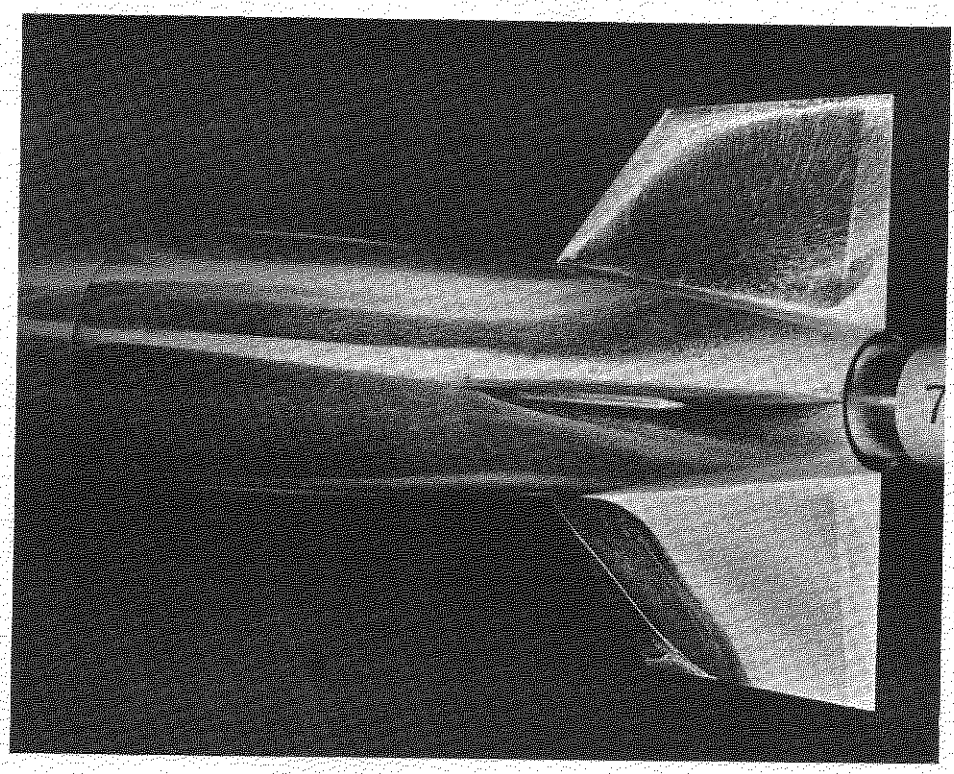

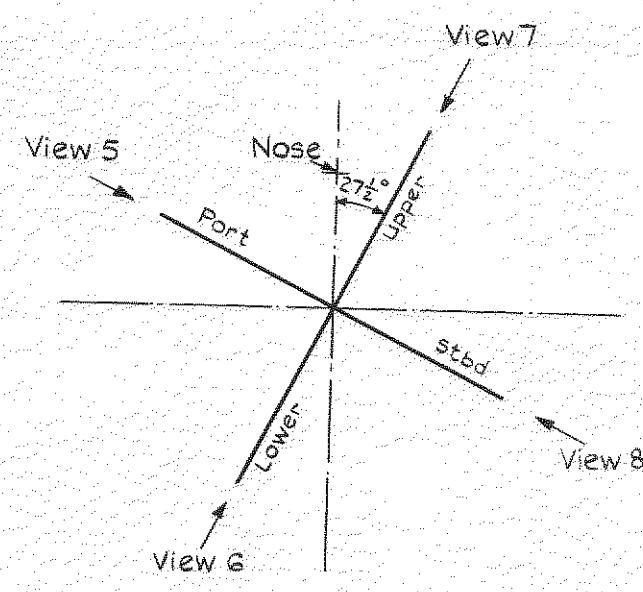

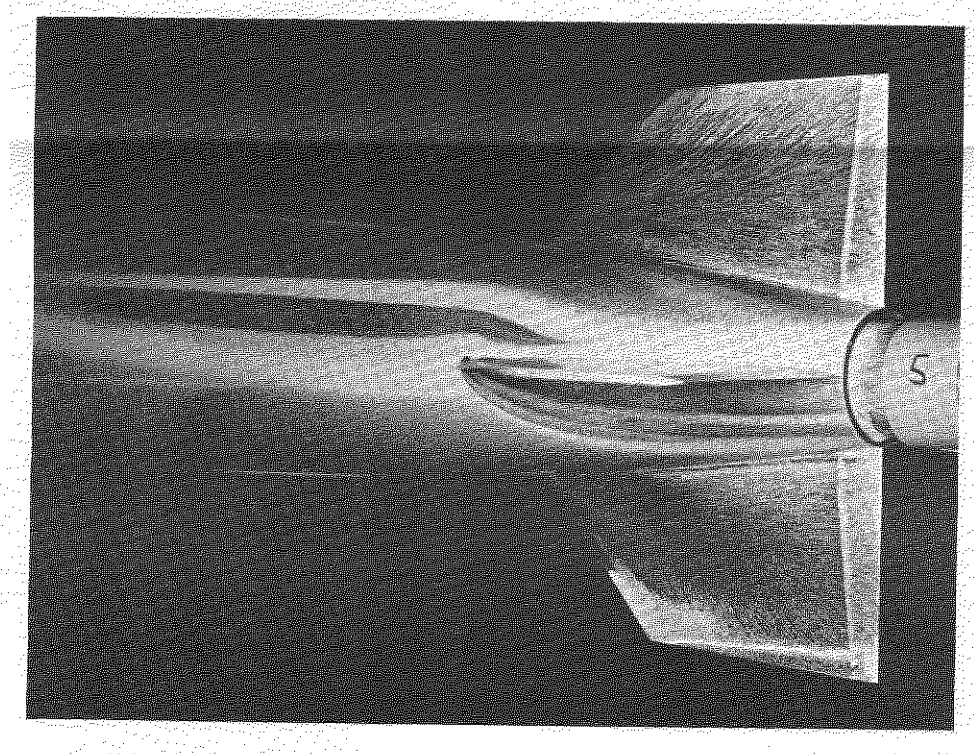

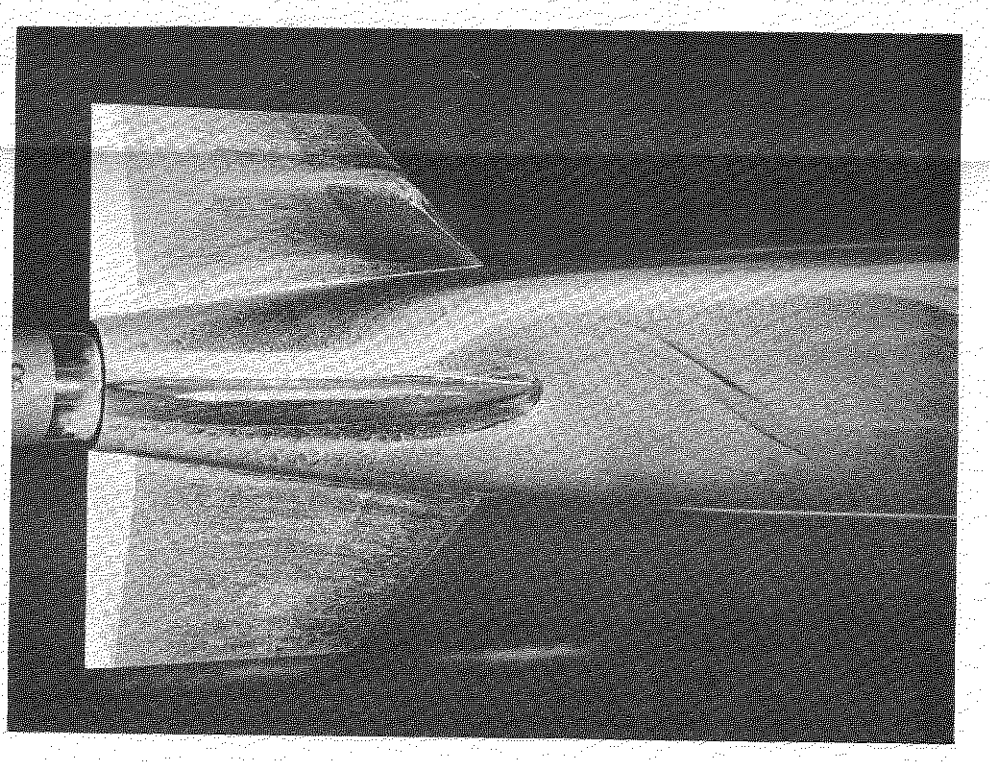

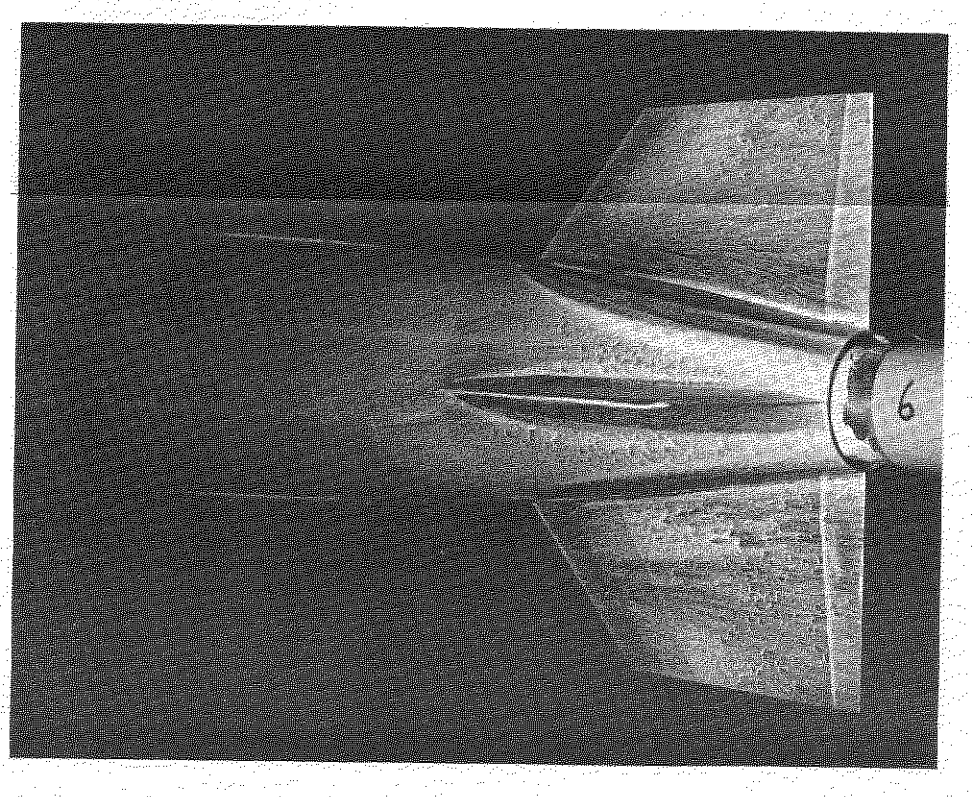

$\sigma = 16.17^{\circ}$ $\lambda = 27.5^{\circ}$ $C_{\ell} = -0.0054$

Fig.16b. Flow visualization.
Pointed nose (1st series of tests)
M=0.50 R=1.29 x 10^6

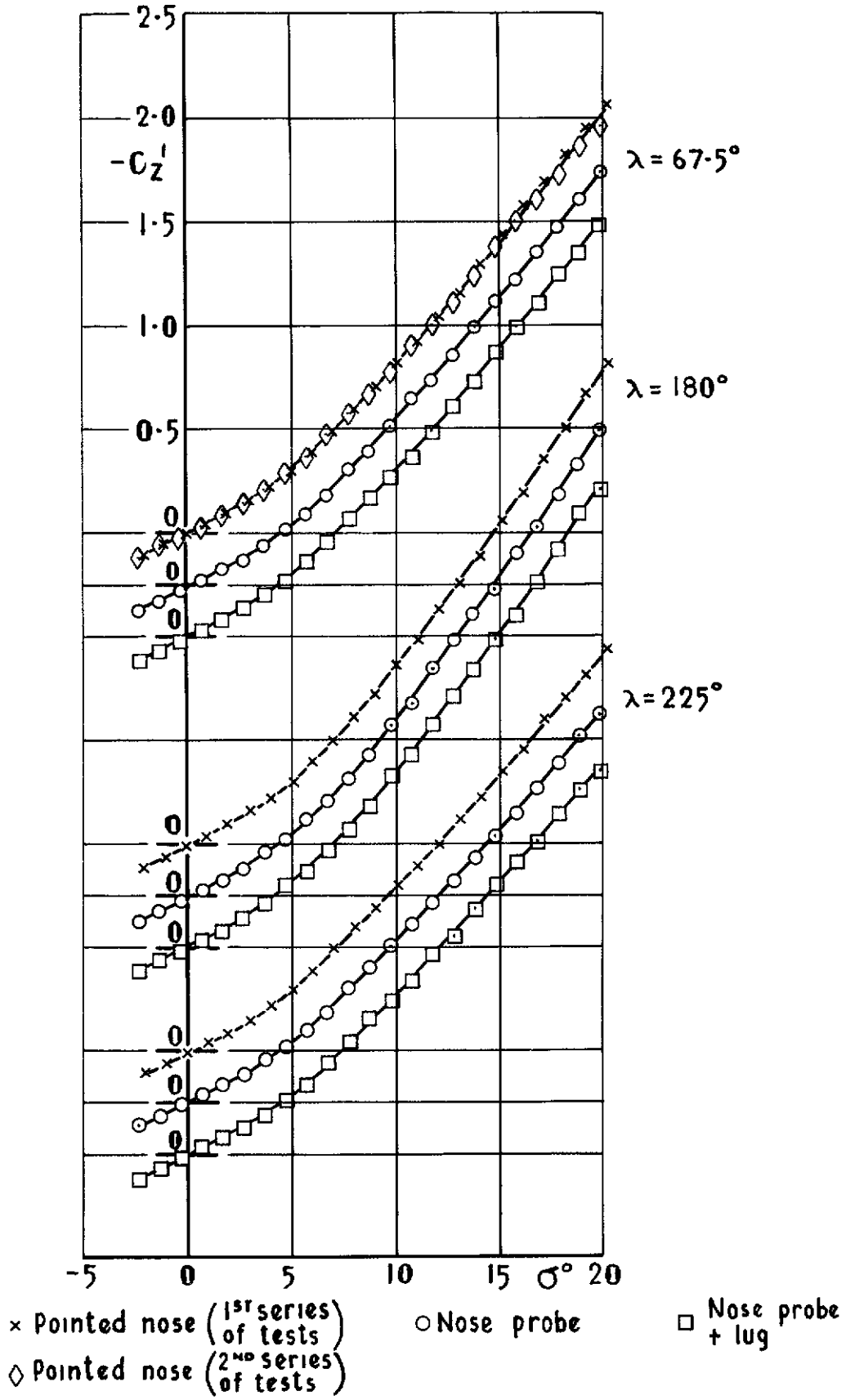

Fig 17b C_z' vs σ, M=0·50, R=1·29×10^6

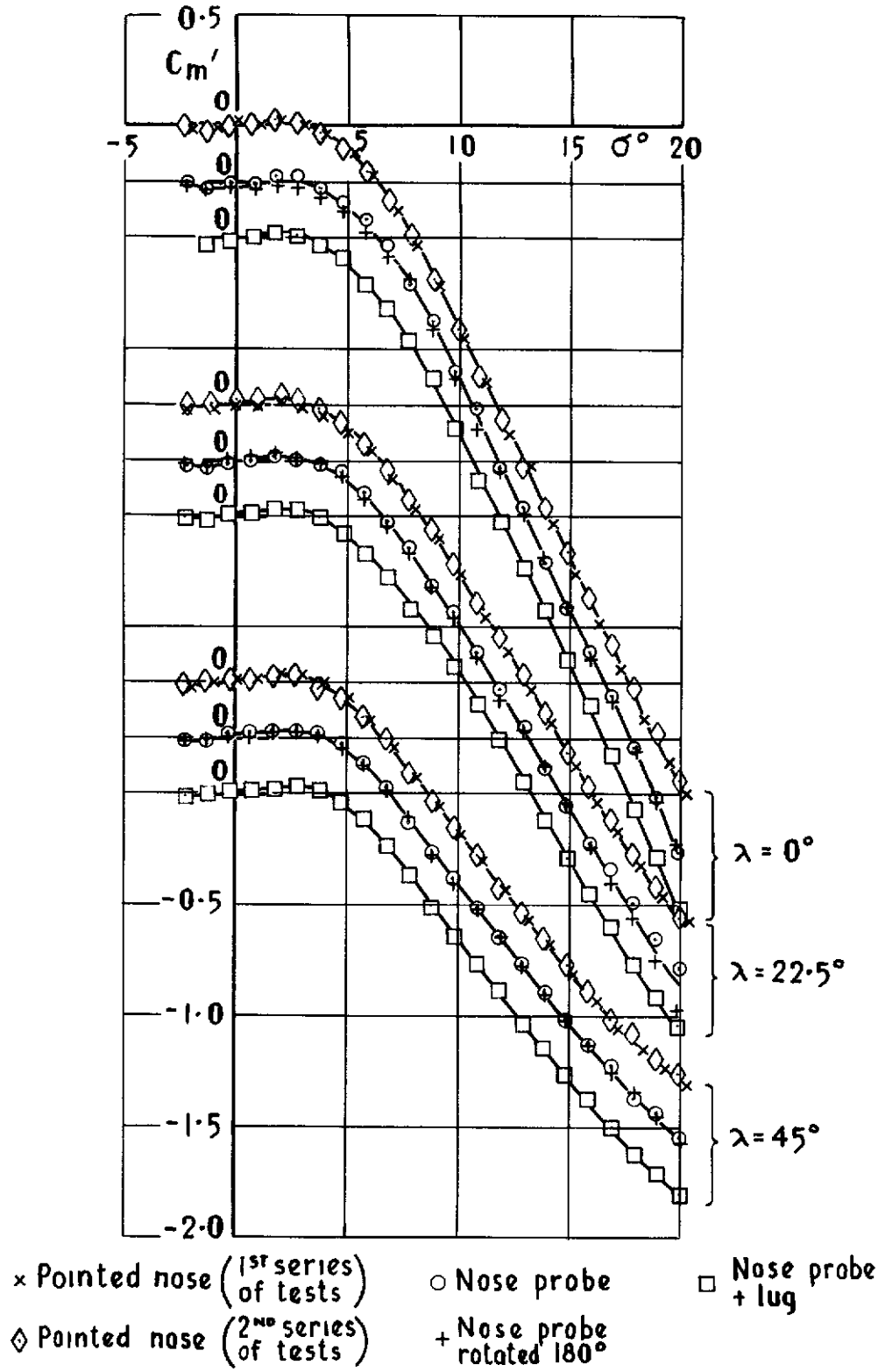

Fig 18a C_m' vs σ, M = 0·50, R = 1·29 × 10^6

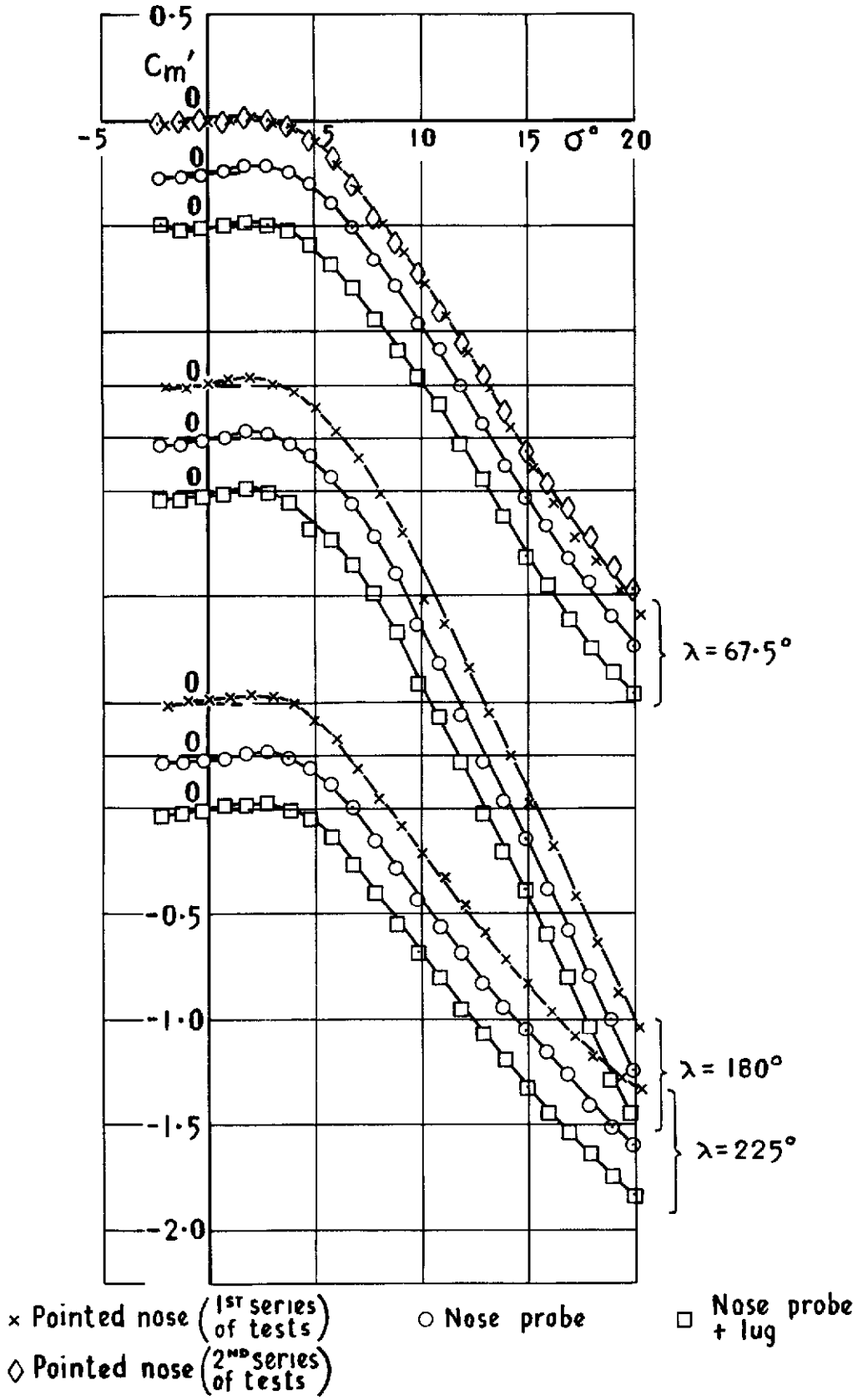

Fig 18b C_m' vs σ, M=0·50, R=1·29x10^6

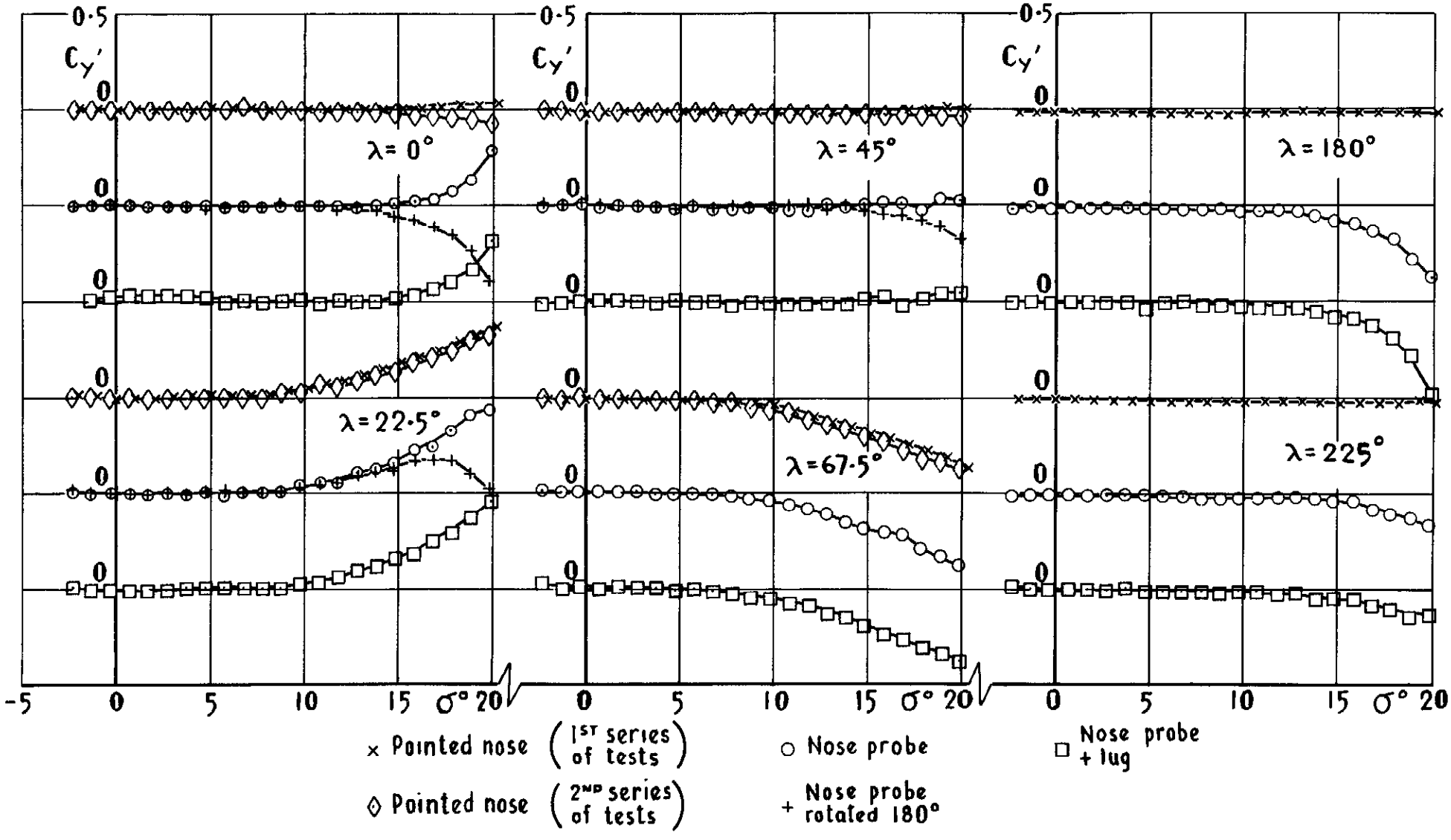

Fig. 19 Cy' vs σ, M=0·50, R=1·29x10⁶

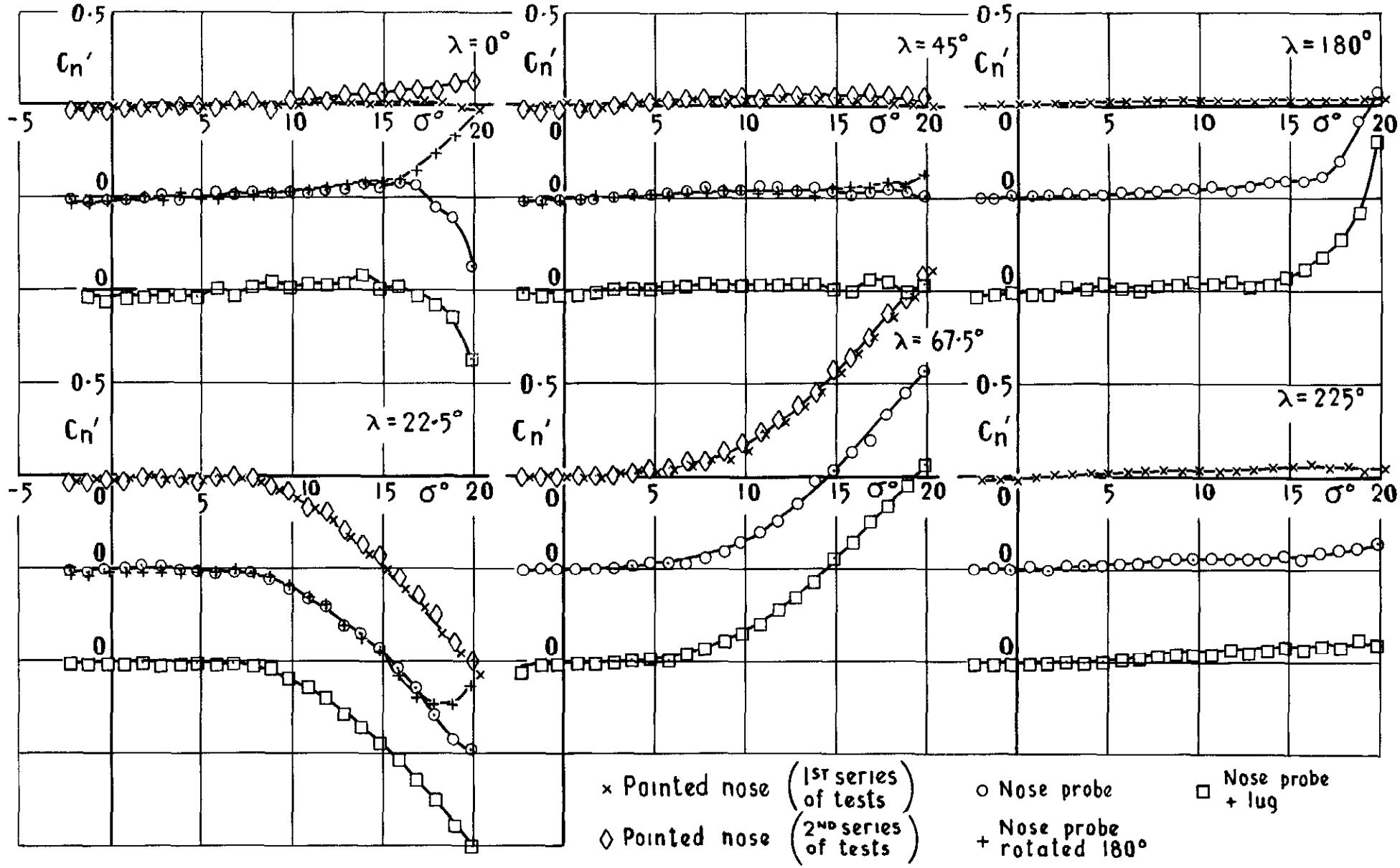

Fig. 20 C_n' vs σ, M=0·50, R=1·29x10^6

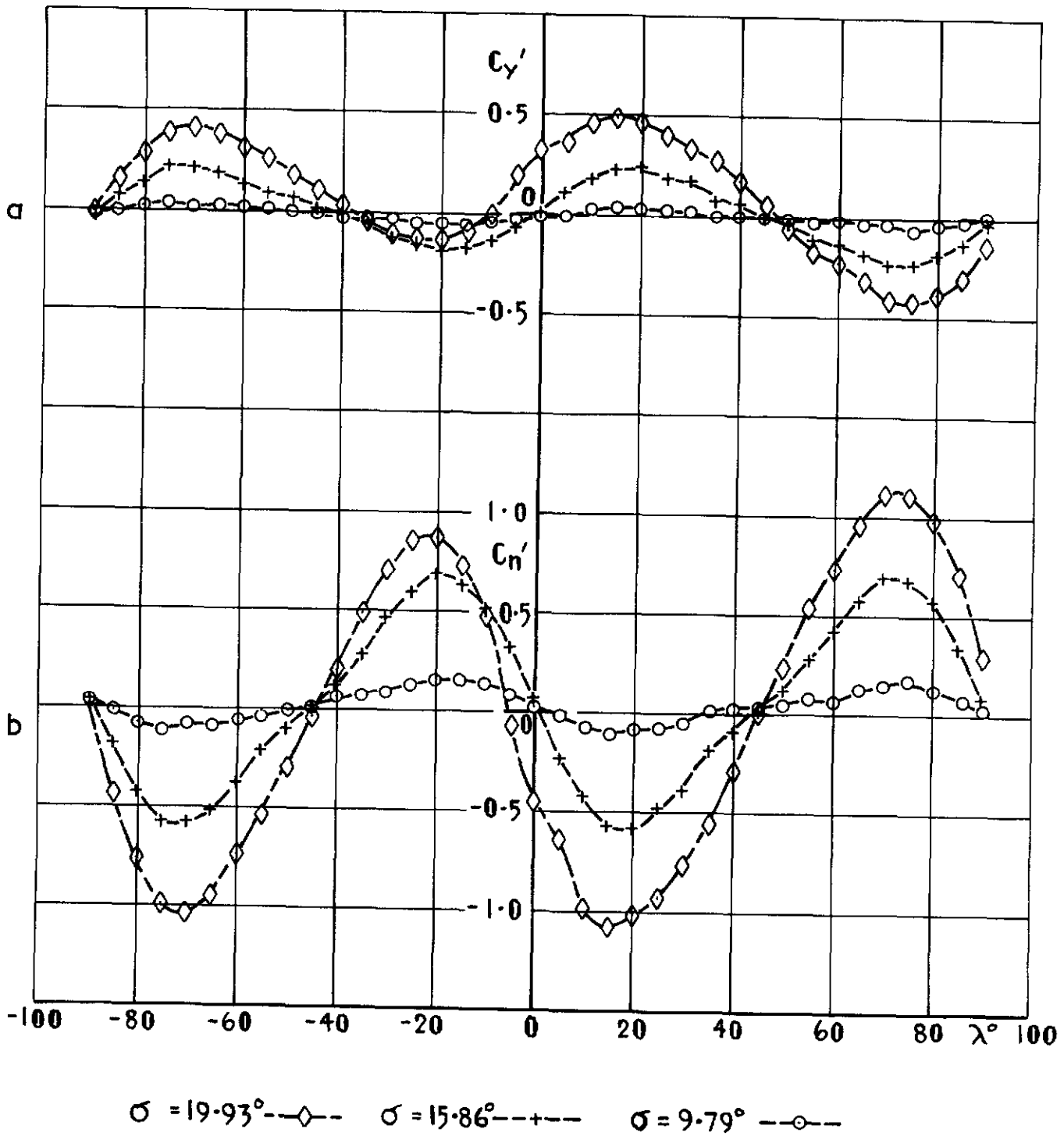

Fig 21 a & b $C_{Y'}$ and $C_{n'}$ vs λ : with nose probe
M=0 50, R=1·29x10^6, λ= -90° to +90°

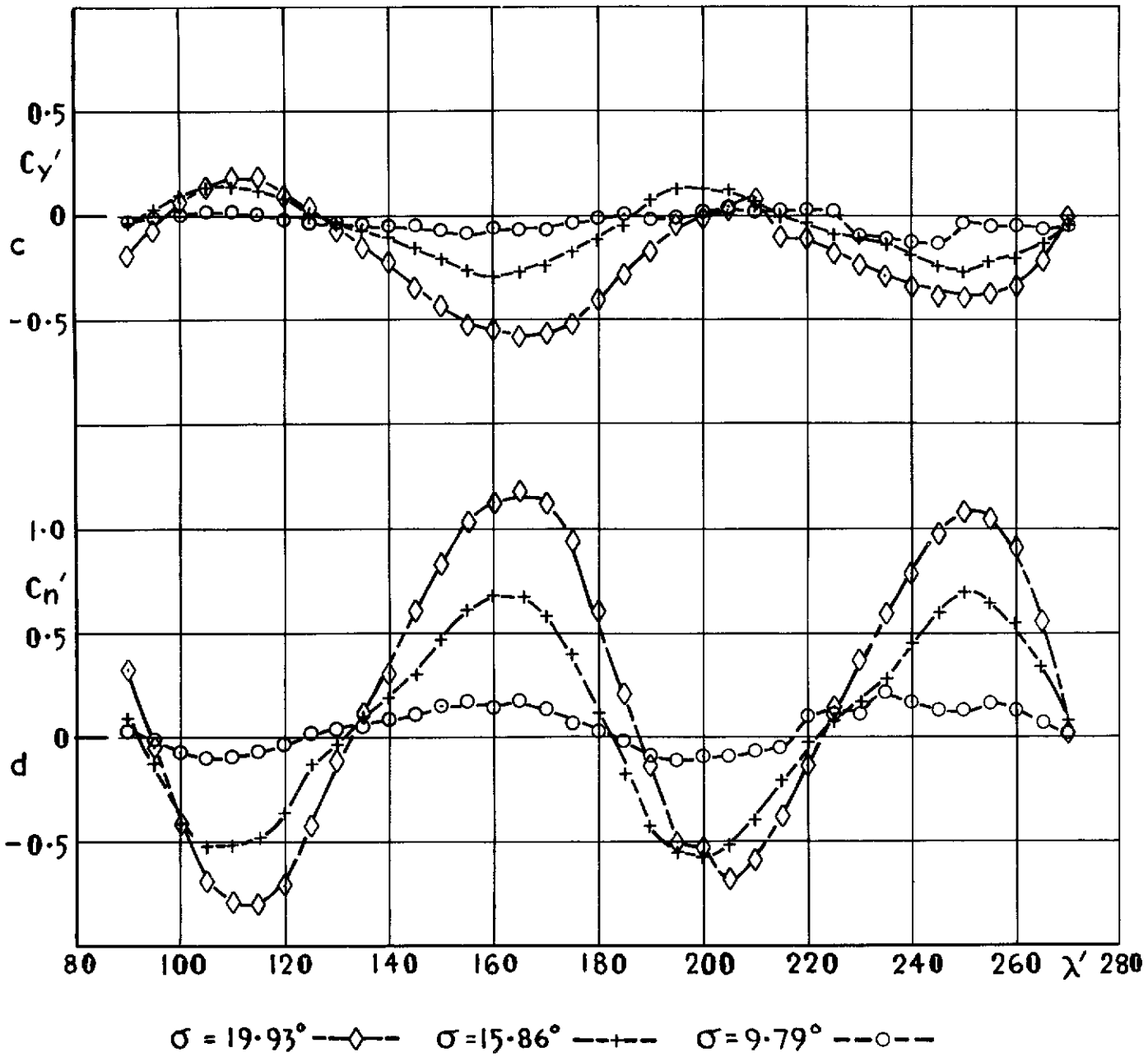

Fig. 21 c & d Cy' and Cn' vs λ : with nose probe
M = 0 50, R = 1 29 x 10⁶, λ = 90° to 270°

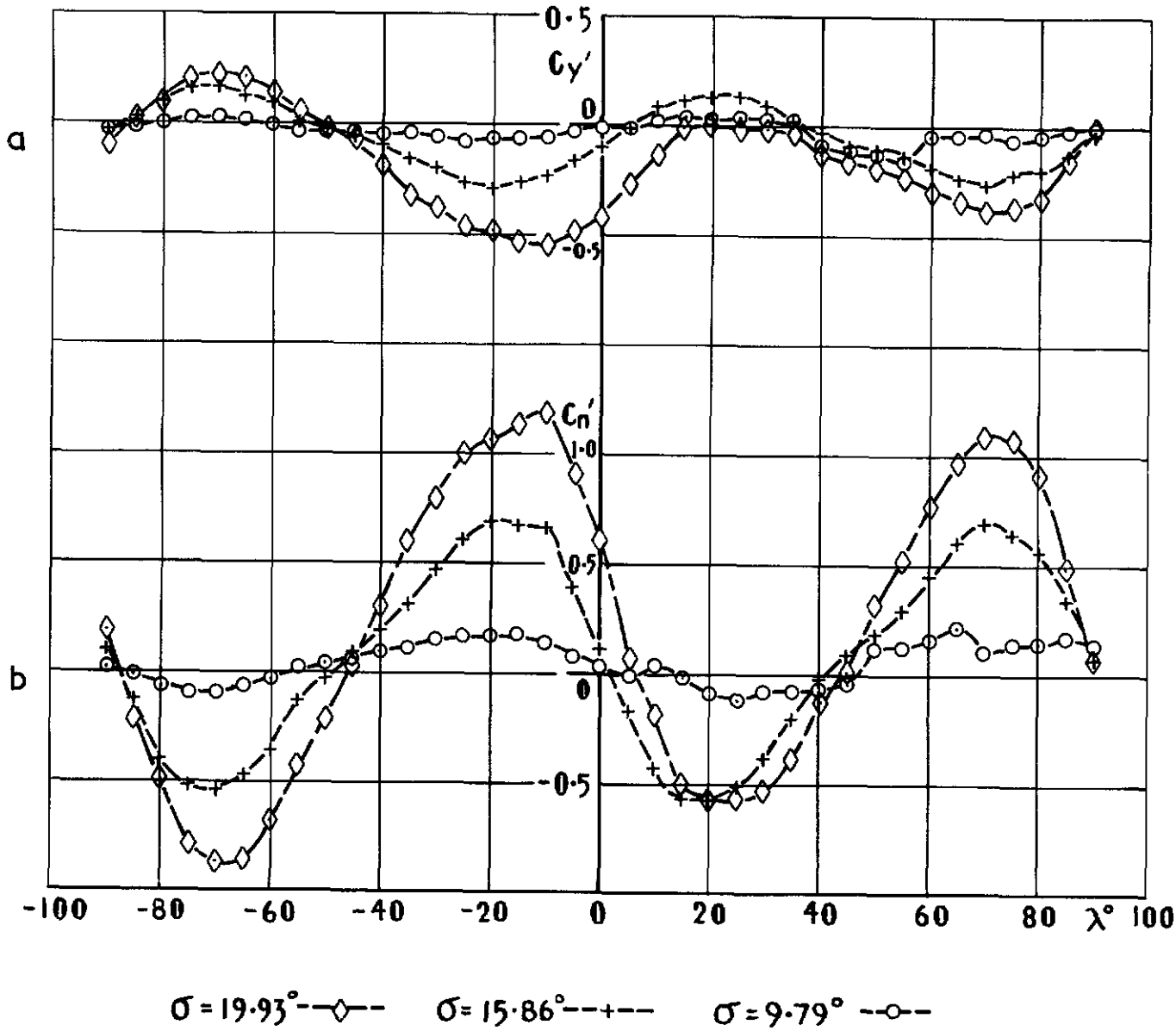

Fig. 22 a & b Cy' and Cn' vs λ: with nose probe rotated 180°
M = 0 50, R = 1·29 x 10⁶, λ = -90° to +90°

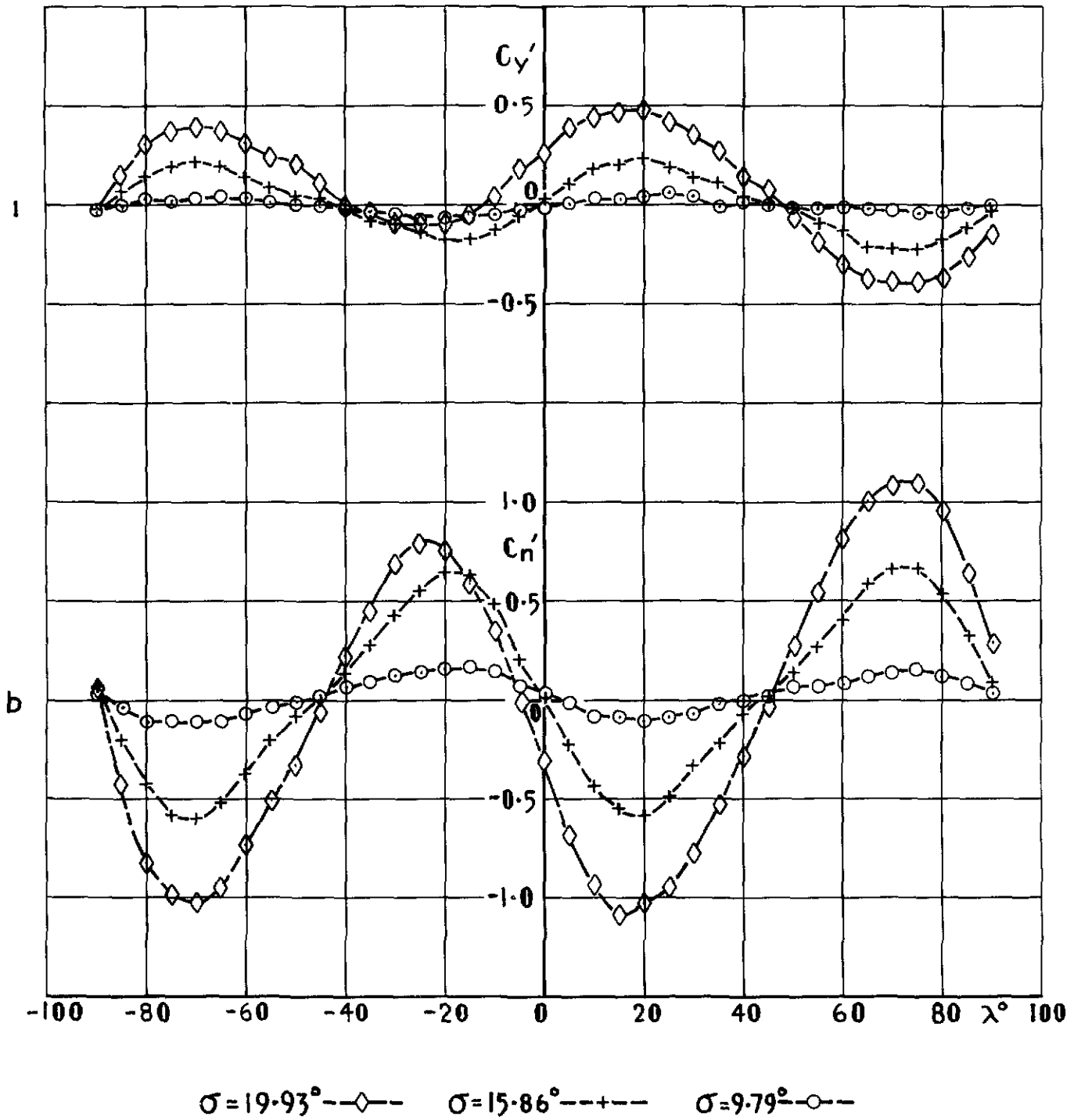

Fig 23a & b Cy' and Cn' vs λ° with nose probe and lug
M=0·50, R=1·29x10^6, λ=-90° to+90°

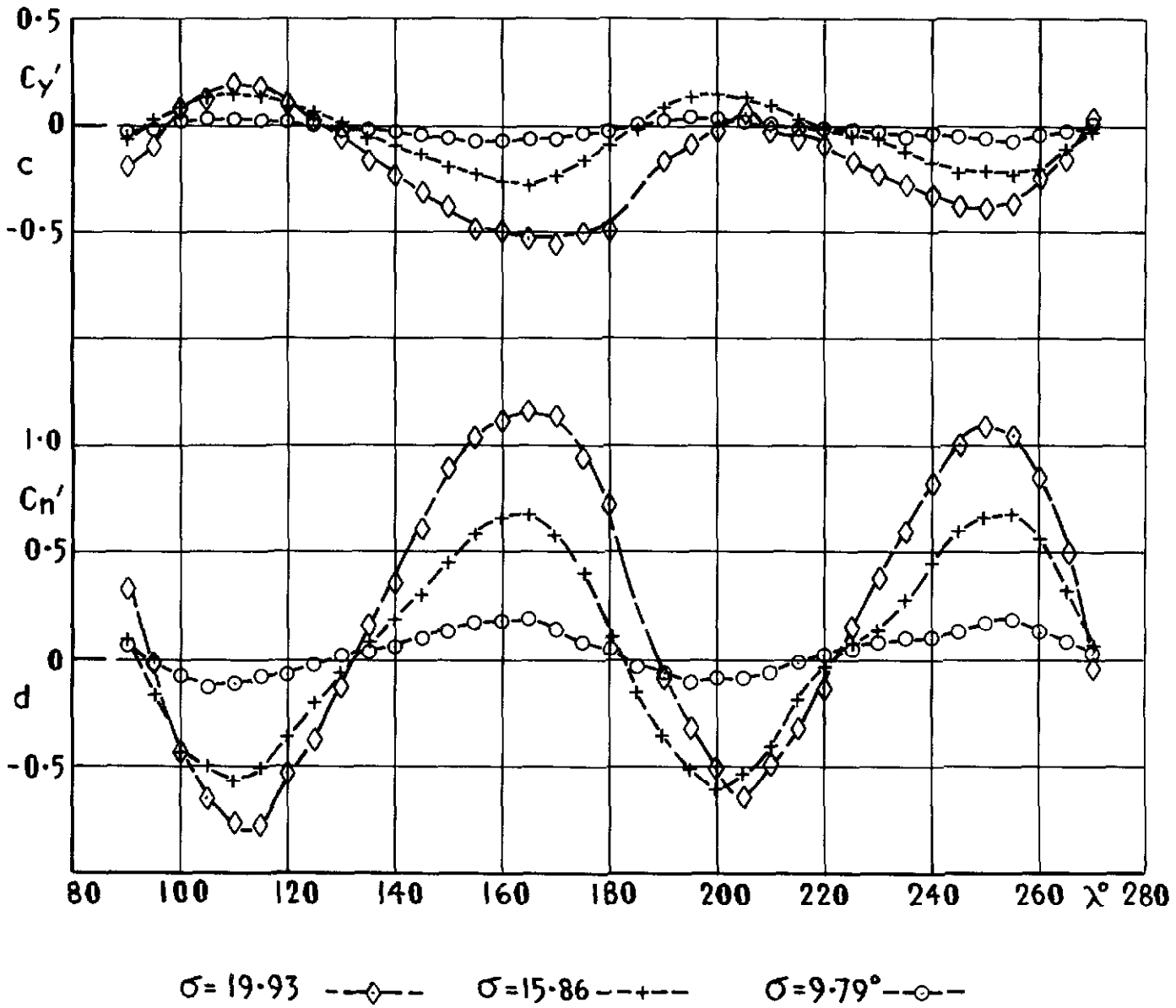

Fig. 23 c & d C_y' and C_n' vs λ : with nose probe + lug
$M = 0{\cdot}50$, $R = 1{\cdot}29 \times 10^6$, $\lambda = 90°$ to $270°$

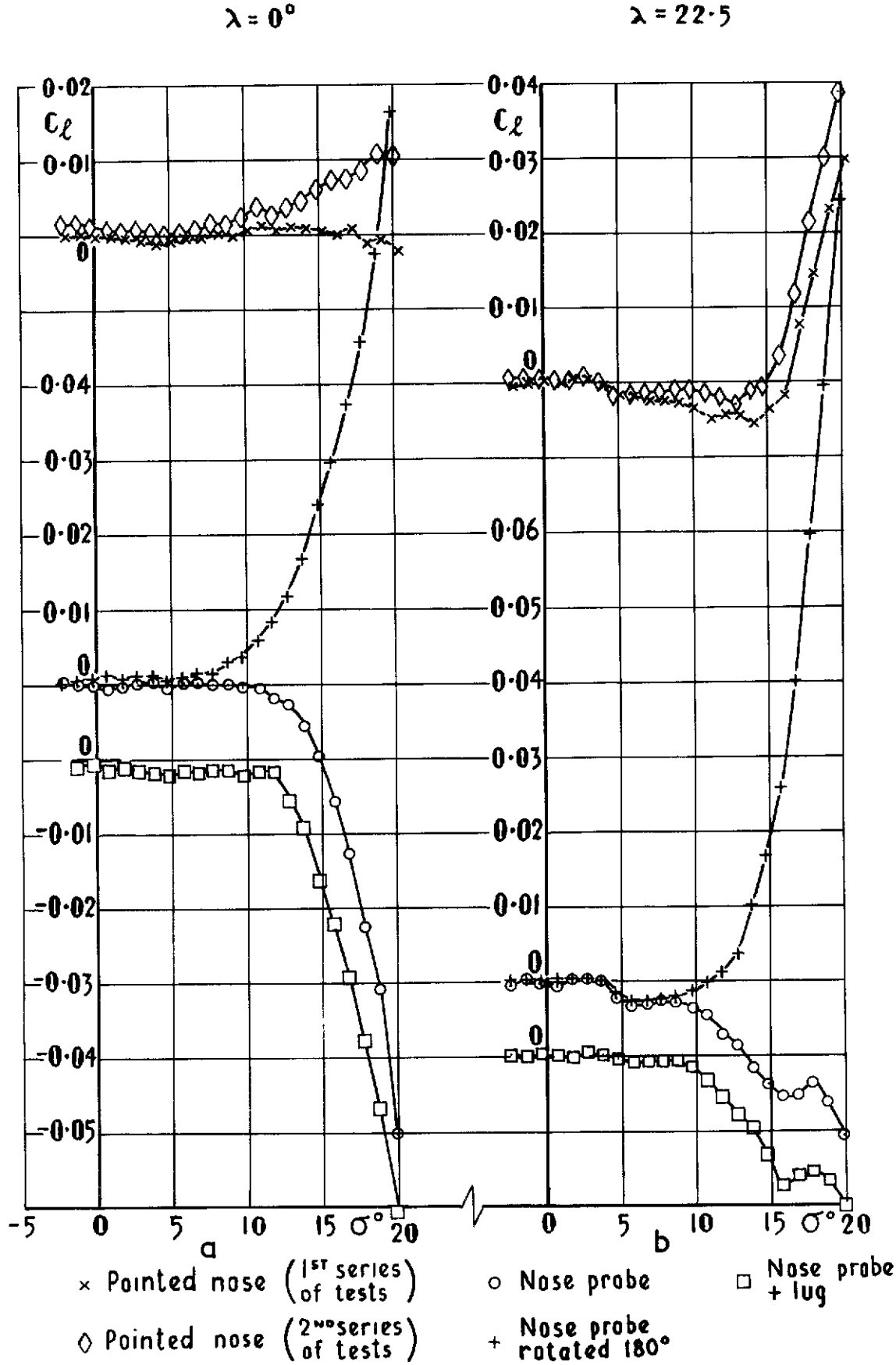

Fig.24a & b C_ℓ vs σ, M=0·50, R=1·29×10⁶

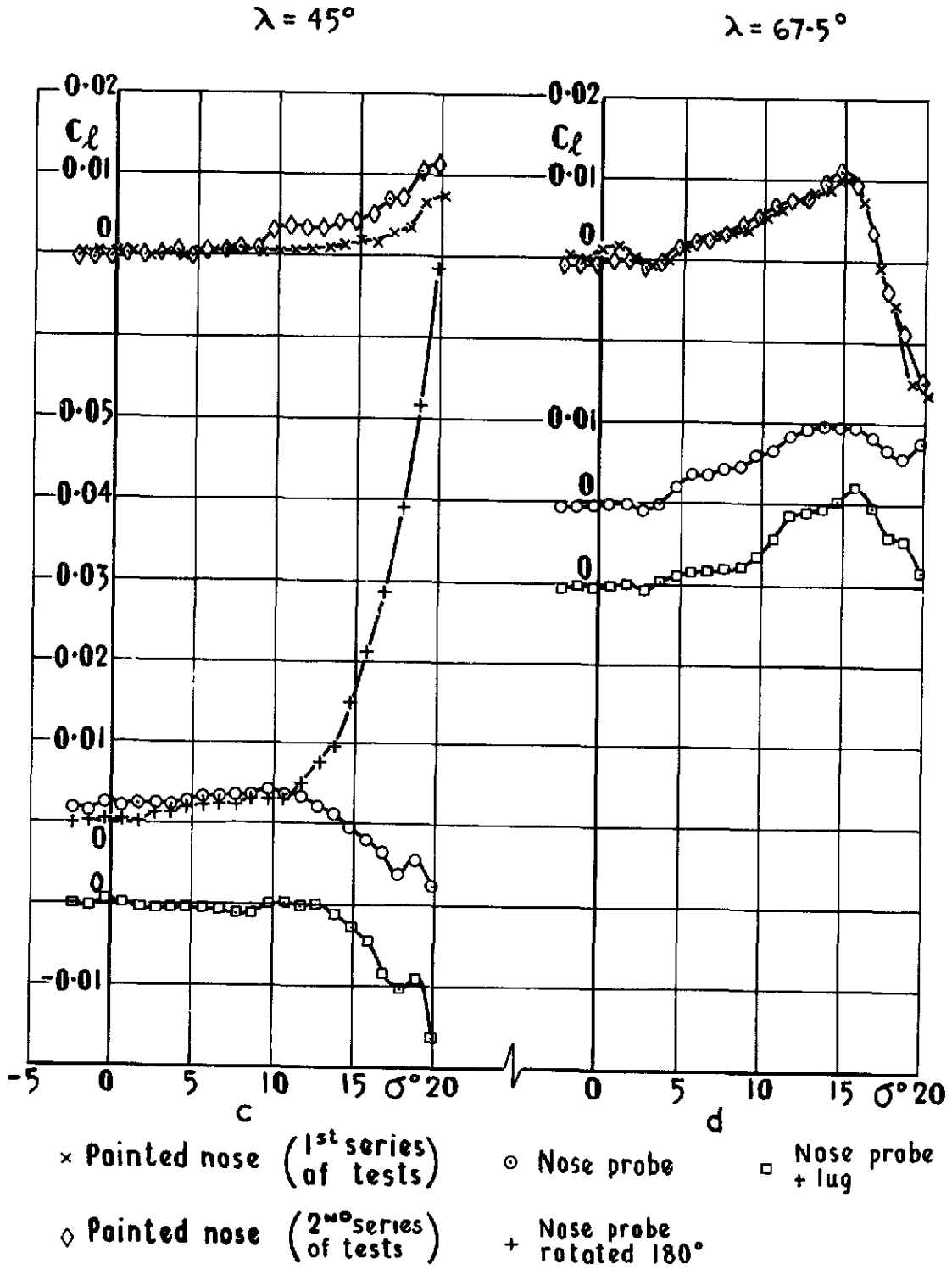

Fig. 24c & d C_ℓ vs σ, M=0·50, R=1·29x10⁶

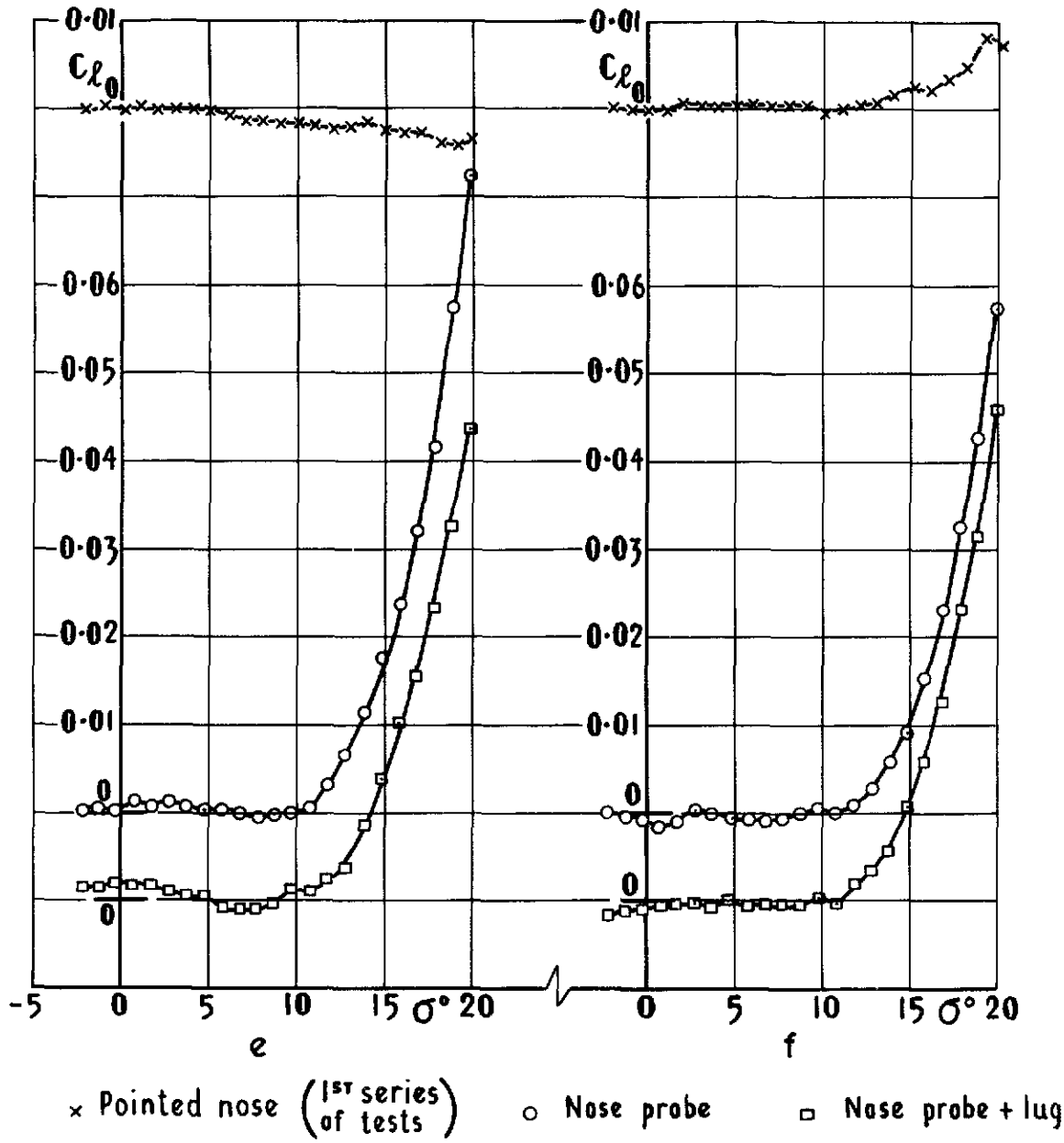

Fig. 24 e & f C_ℓ vs σ, M = 0·50 , R = 1 29 x 10^6

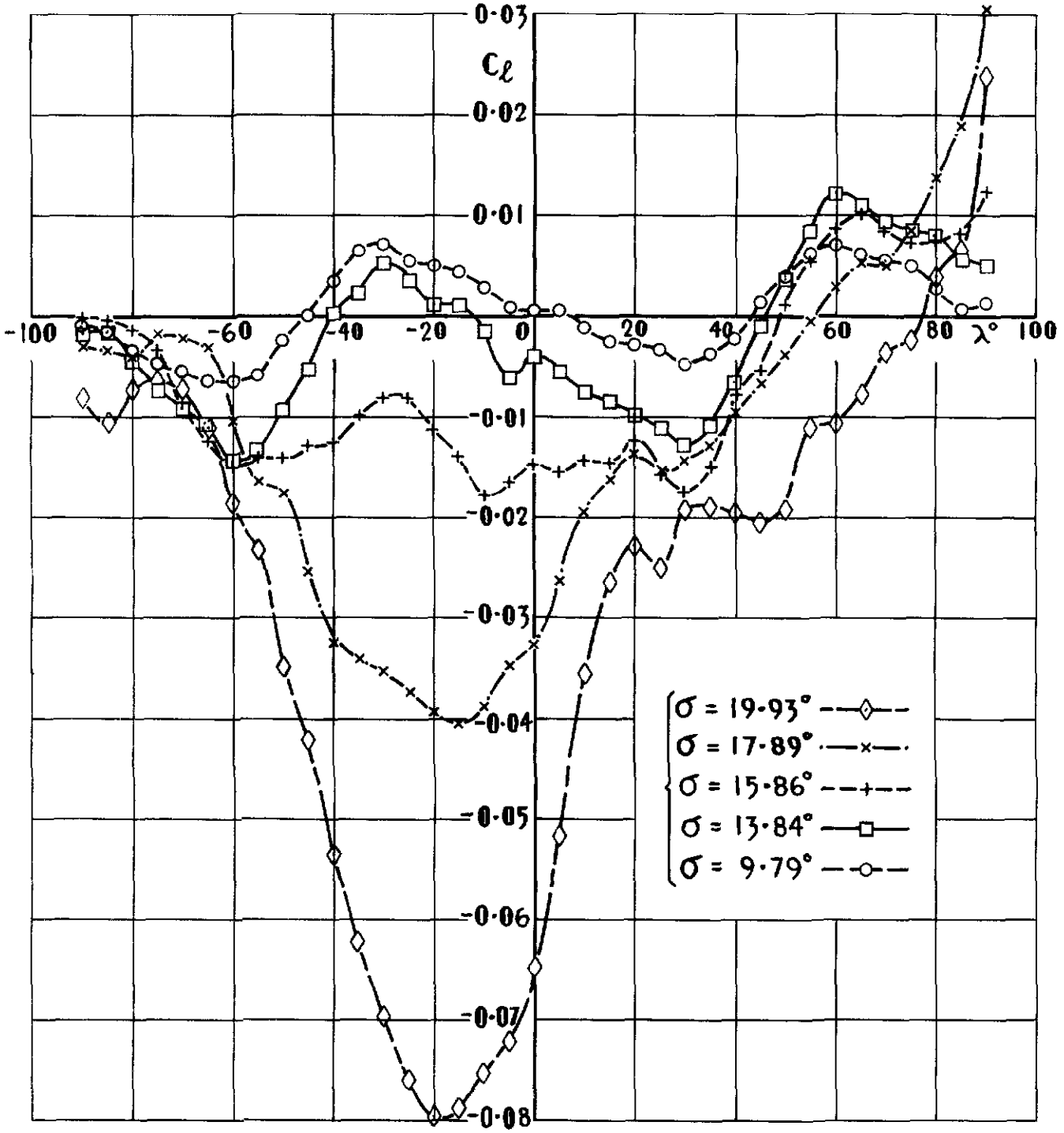

Fig.25a C_ℓ vs λ, M=0 50, R=1·29 x 10^6 with nose probe
$\lambda = -90°$ to $+90°$

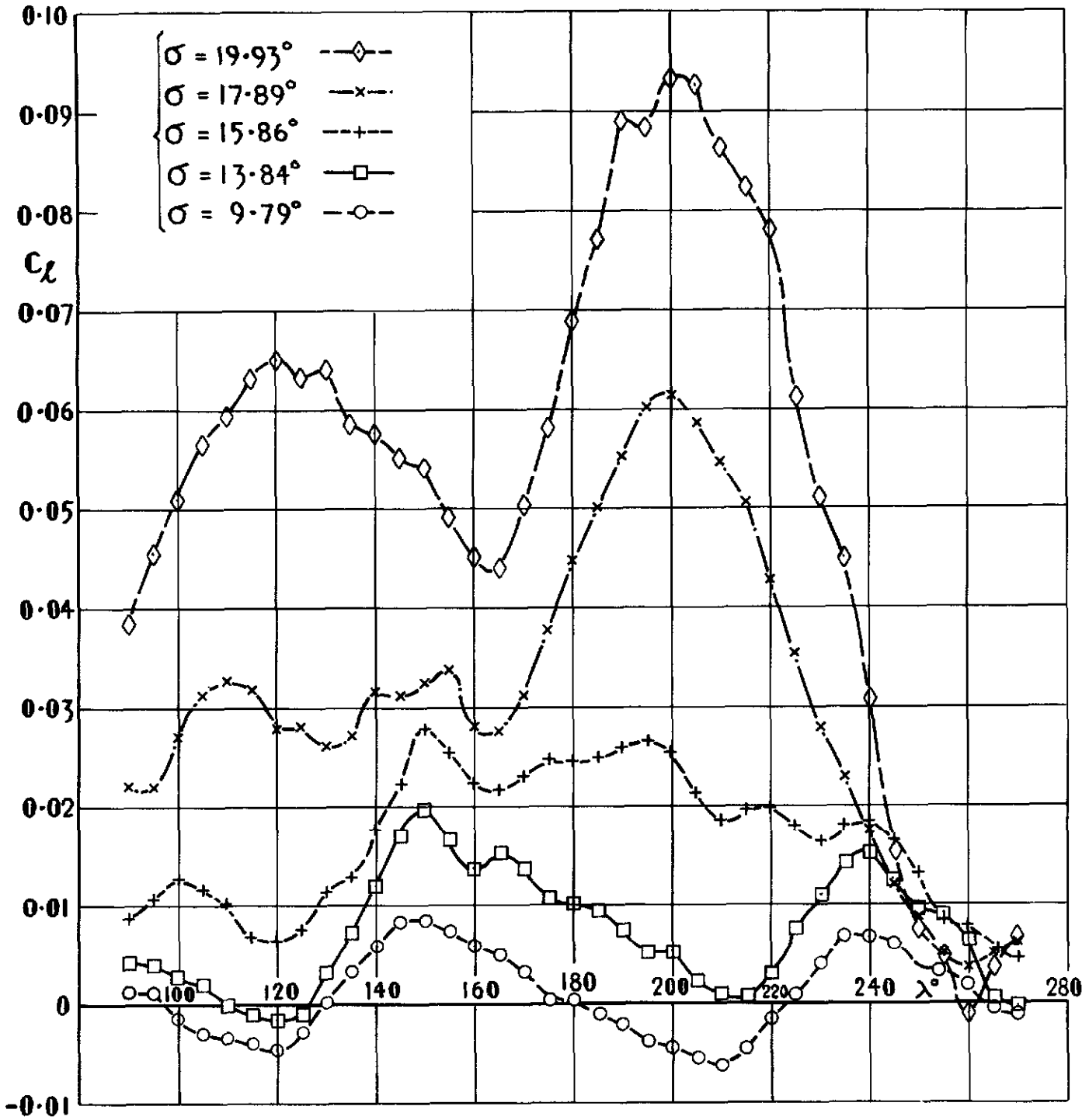

Fig.25b C_ℓ vs λ , M=0 50 , R=1·29 x 10^6 with nose probe
λ = 90° to 270°

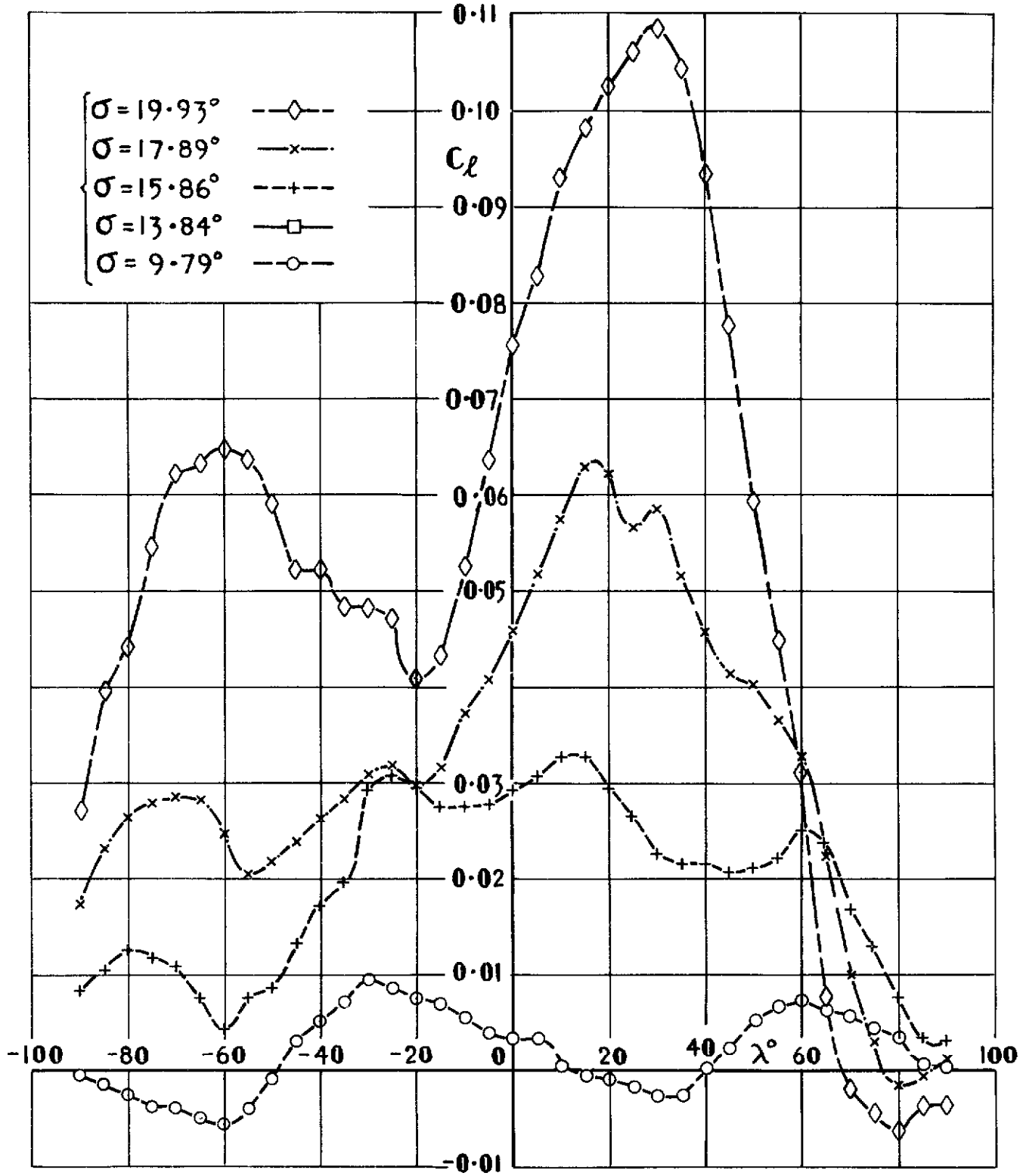

Fig. 26 C_ℓ vs λ, M=0·50, R=1·29 x 10^6 with nose probe rotated 180°
$\lambda = -90°$ to $+90°$

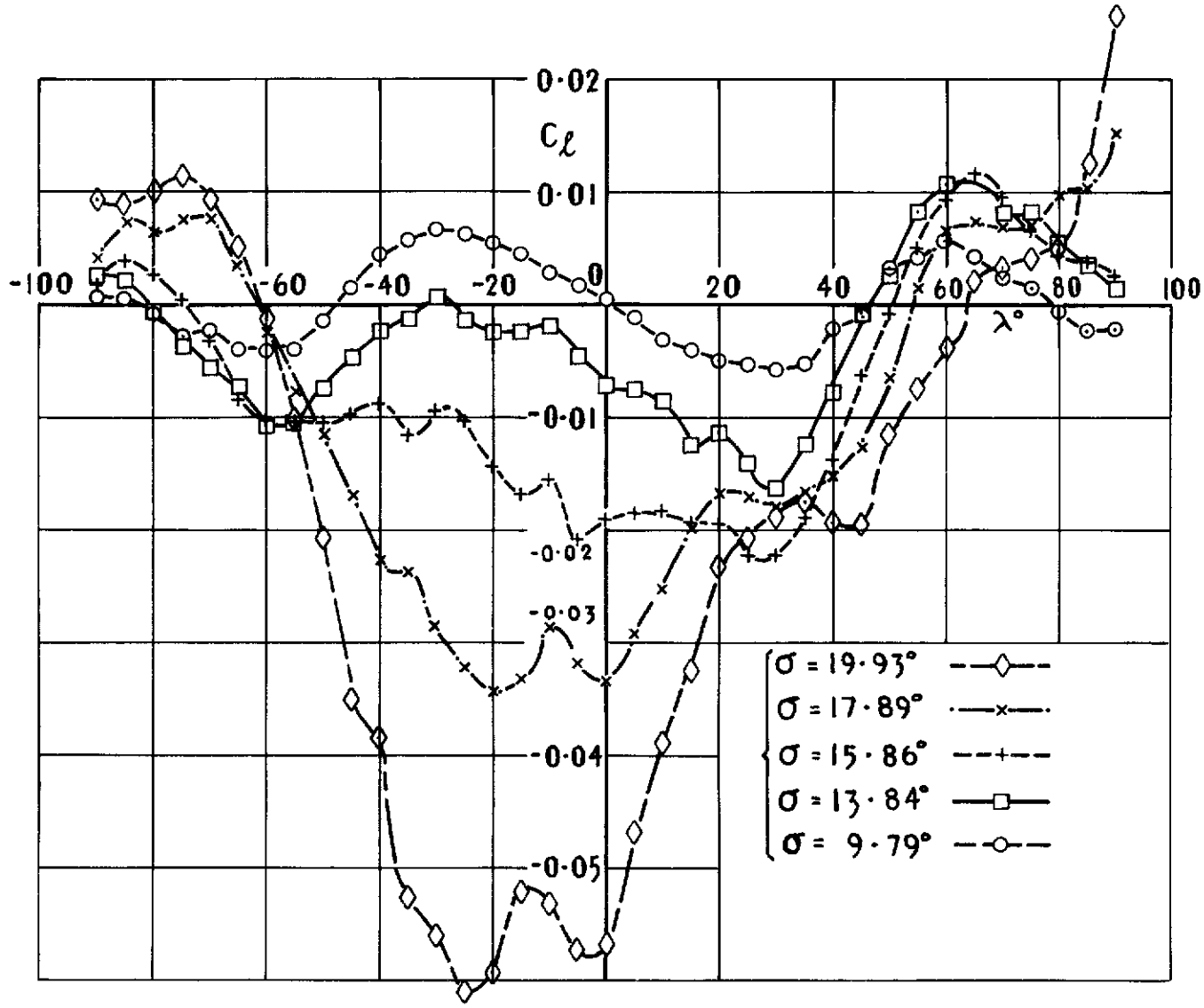

Fig. 27a C_ℓ vs λ, M=0·50, R=1·29 x 10^6 with nose probe + lug

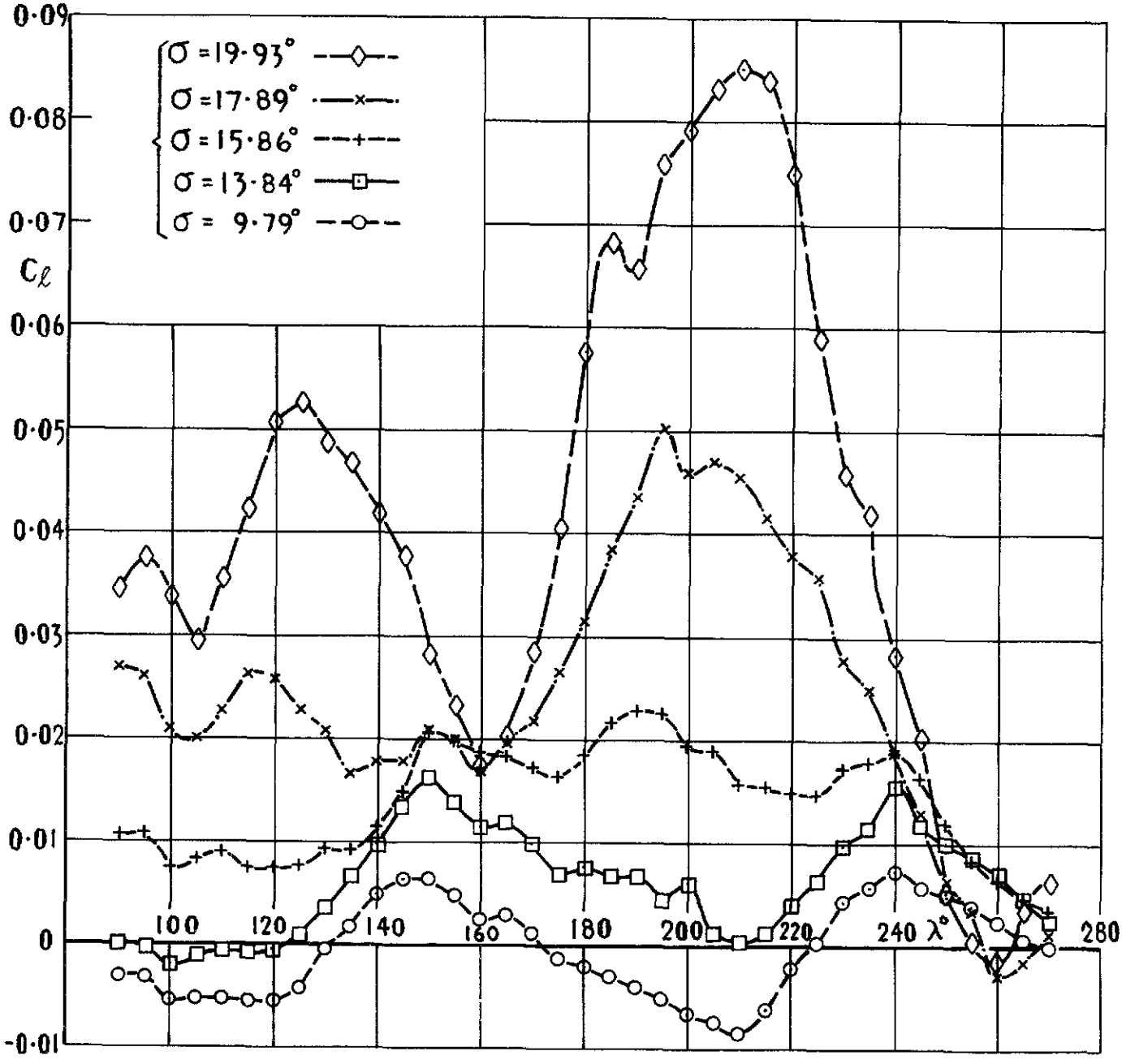

Fig 27b C_ℓ vs ϕ, M=0·50, R=1·29 x 10^6 with nose probe + lug
λ = 90° to 270°

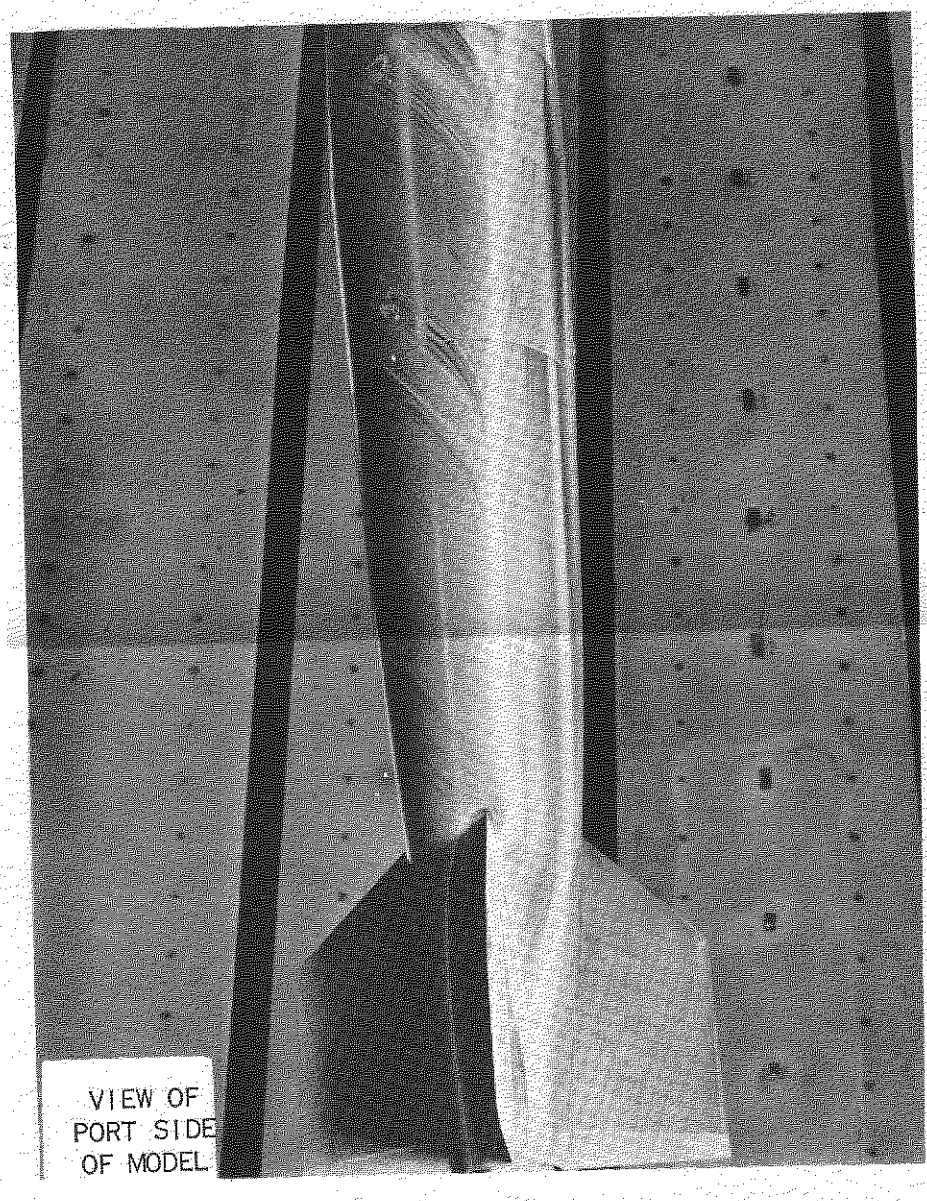

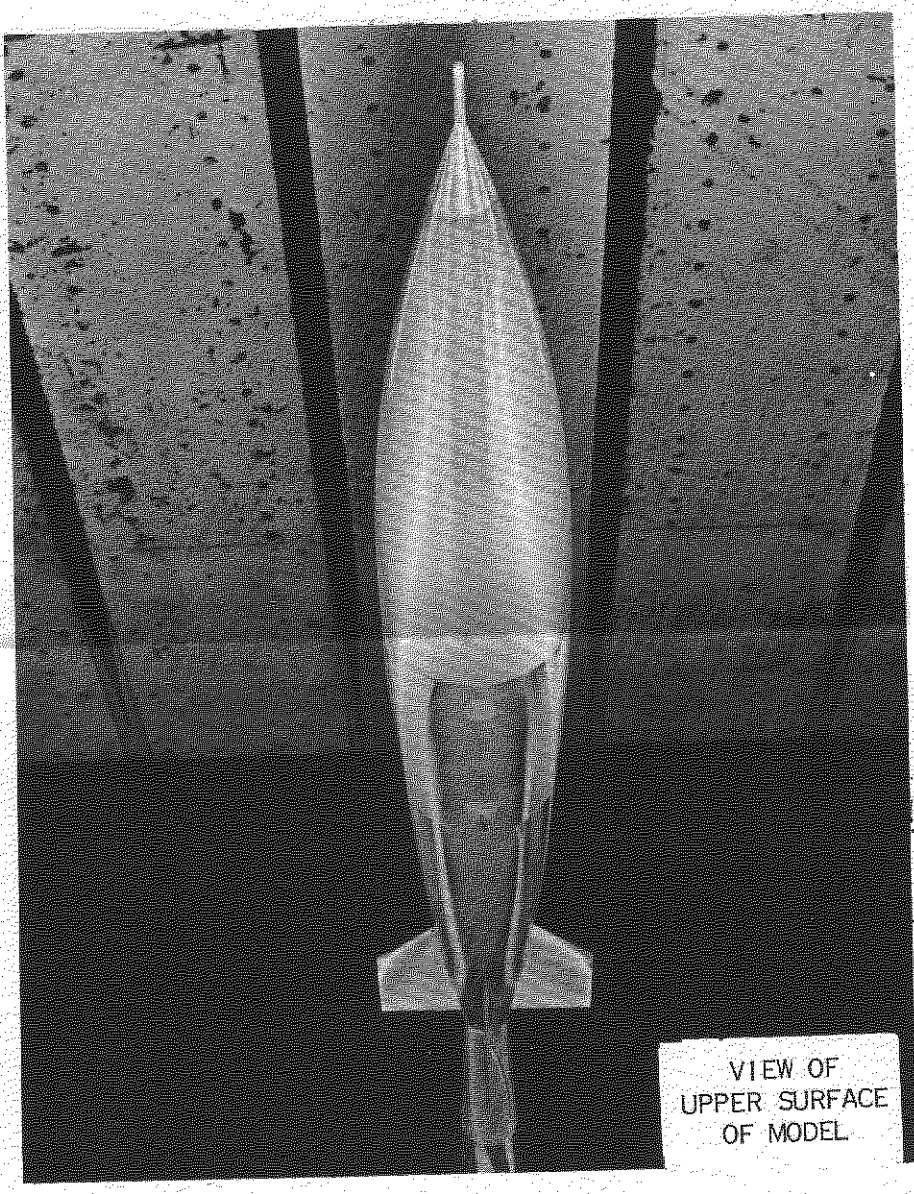

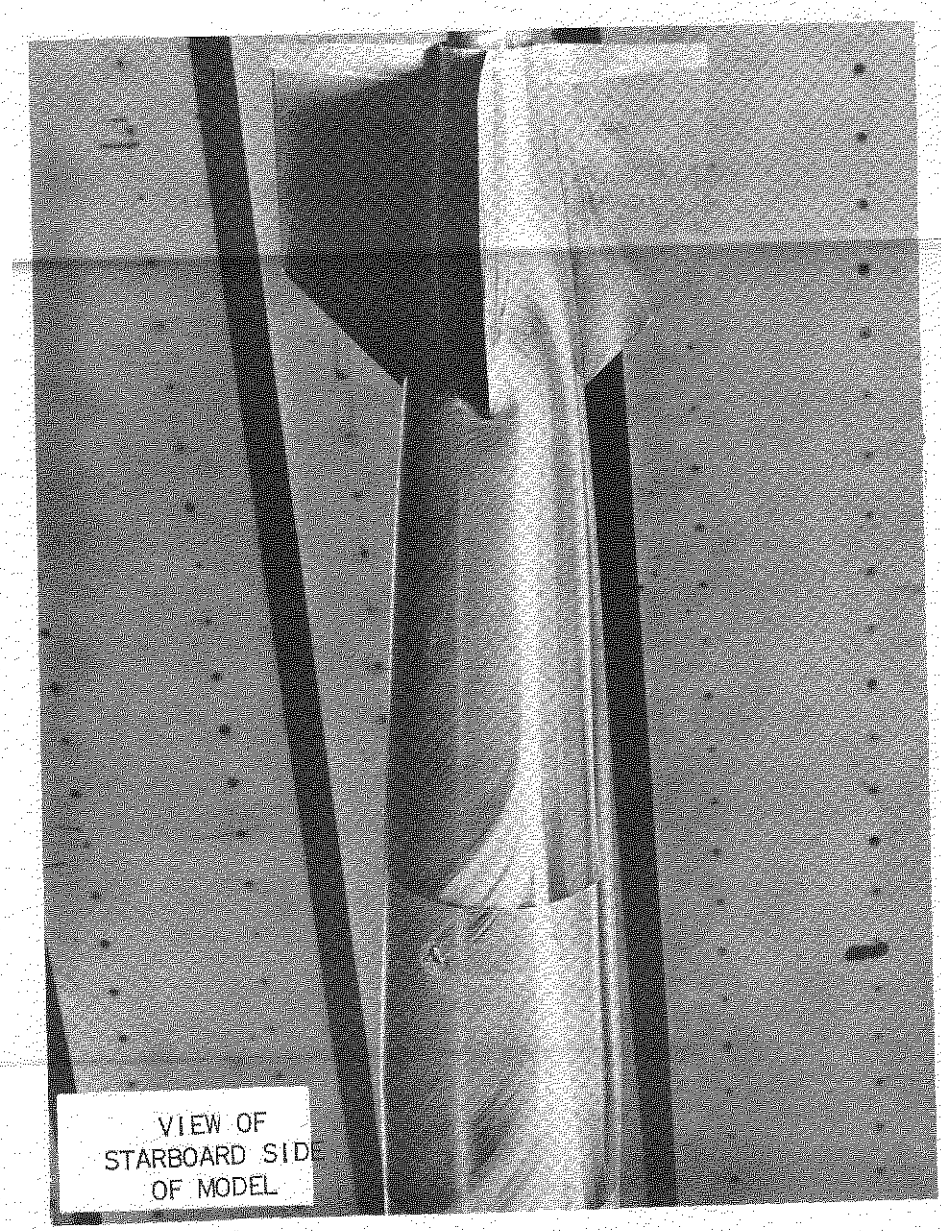

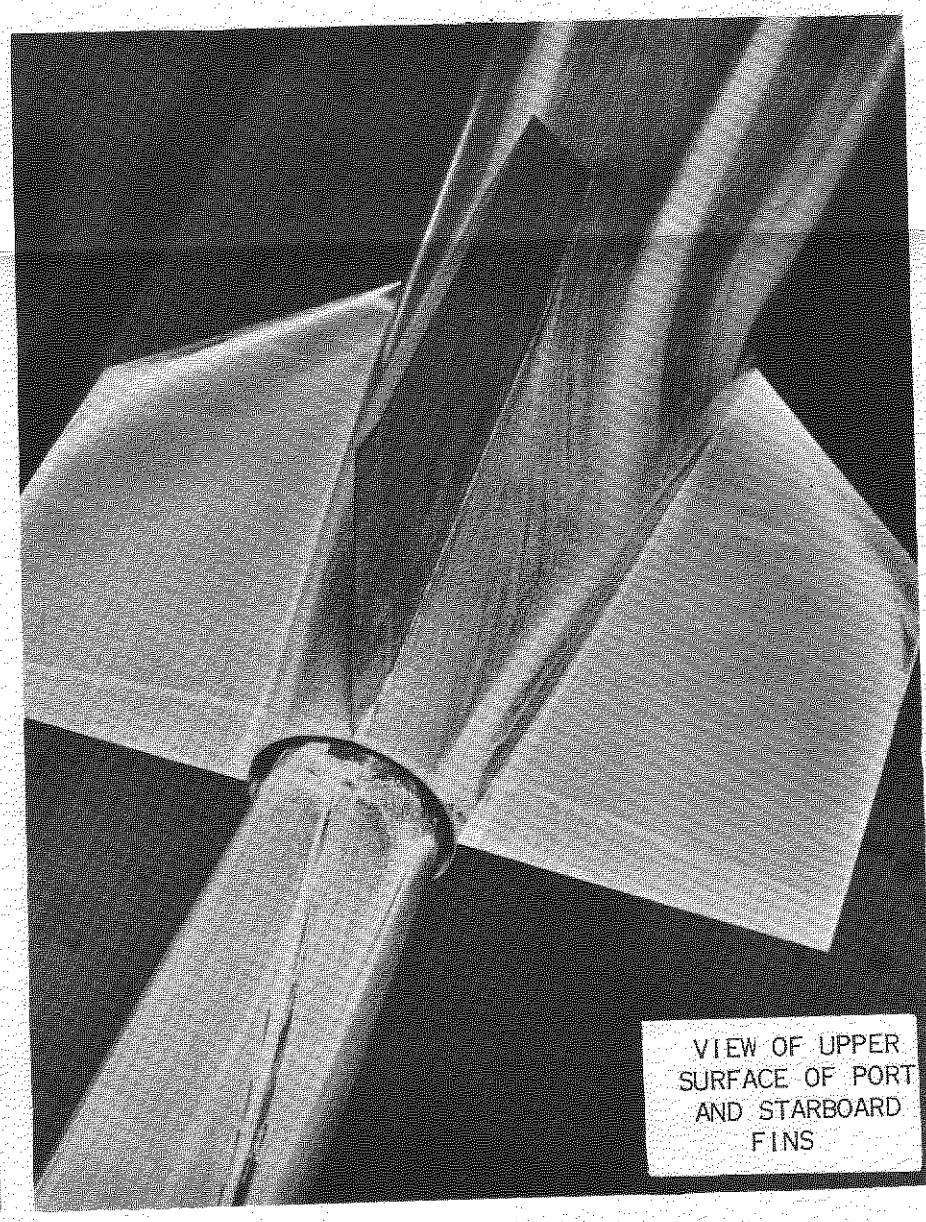

Fig.28a. Flow visualization. Model with nose probe.

$\sigma = 19.93^{\circ}$ $\lambda = 0^{\circ}$ $M = 0.50$ $R = 1.29 \times 10^{6}$

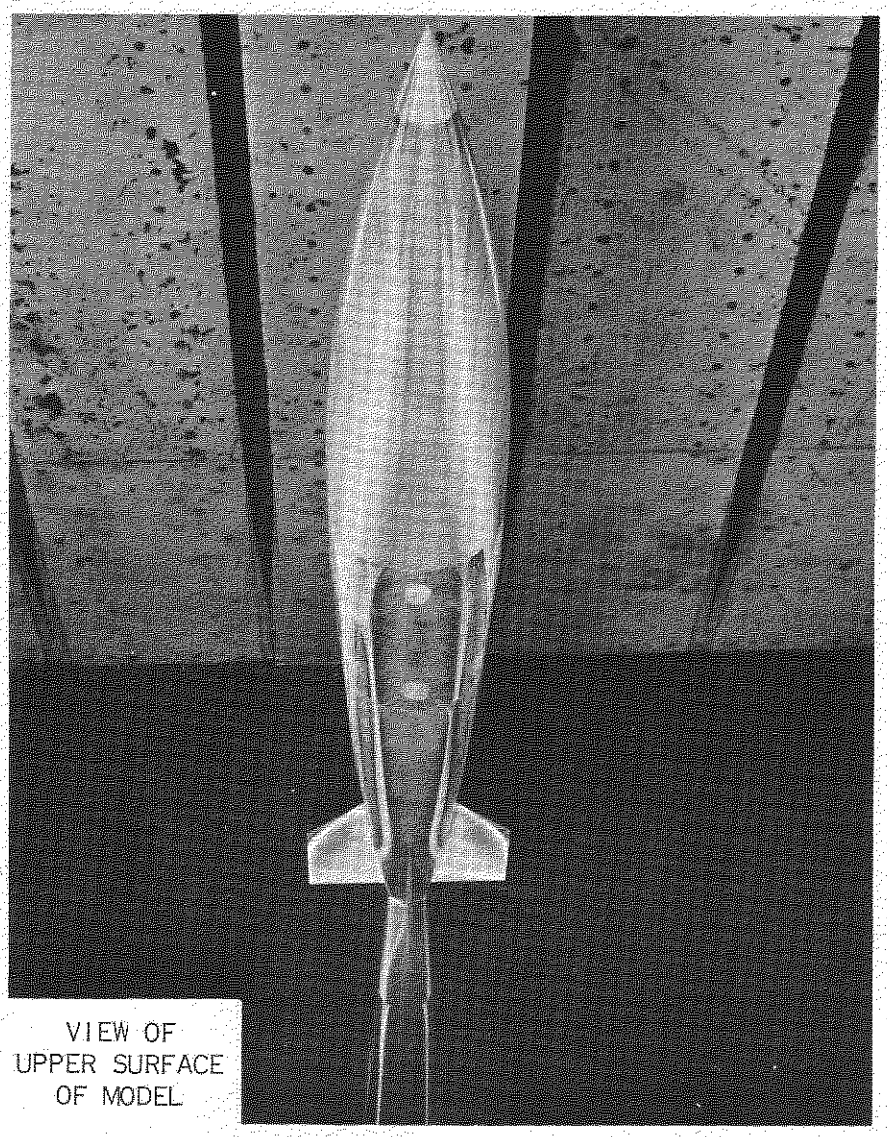

VIEW OF
UPPER SURFACE
OF MODEL

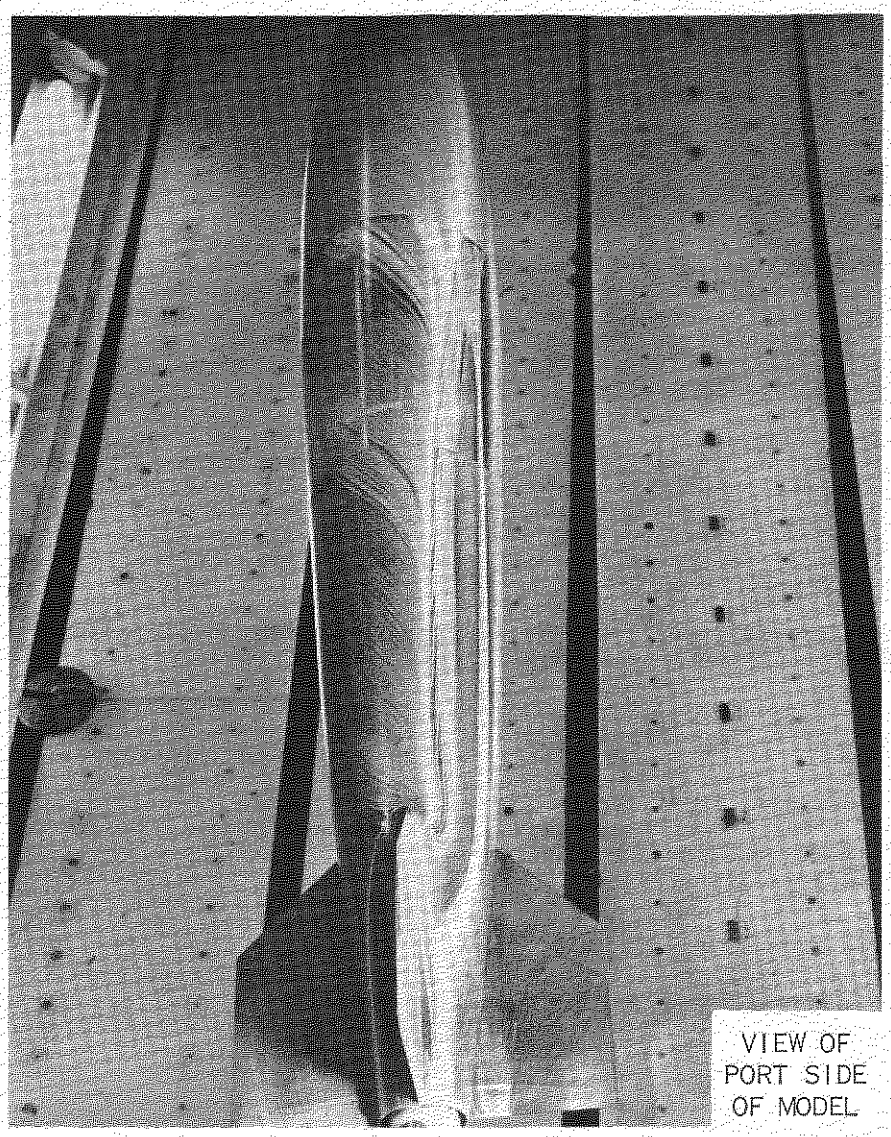

VIEW OF
PORT SIDE
OF MODEL

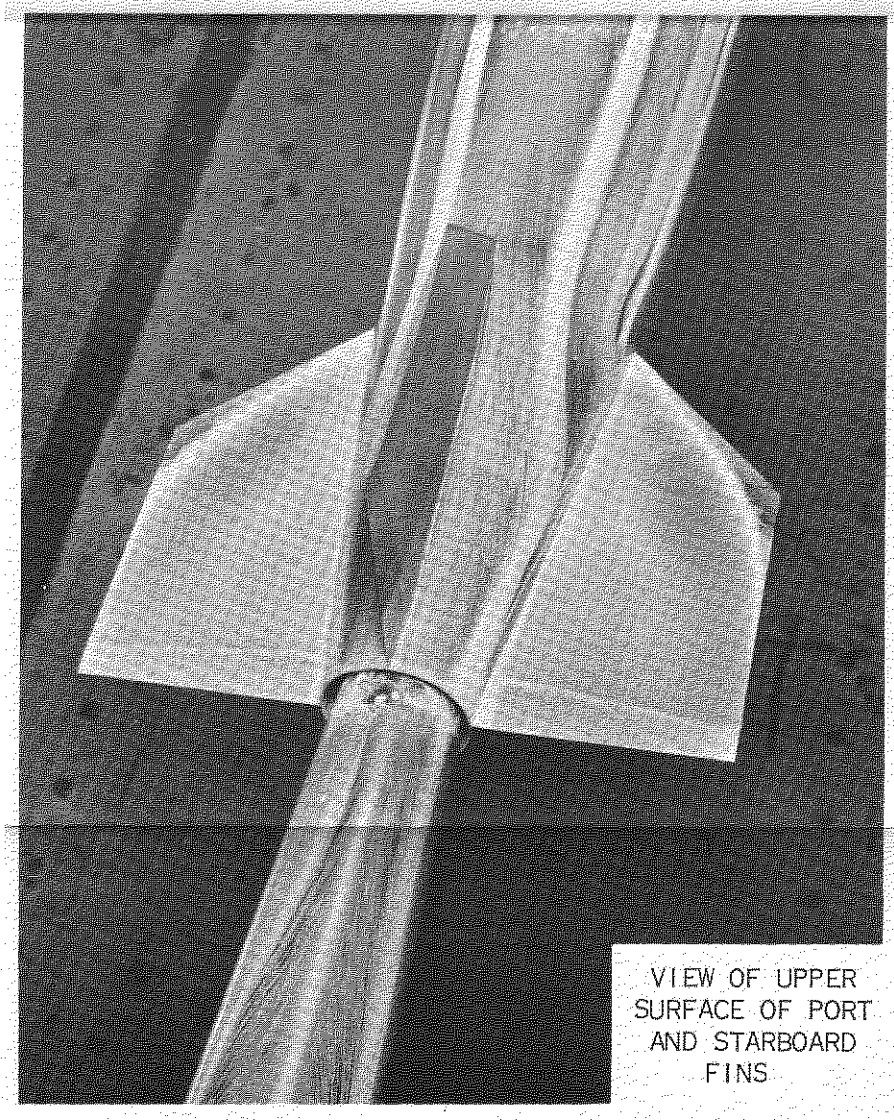

VIEW OF UPPER
SURFACE OF PORT
AND STARBOARD
FINS

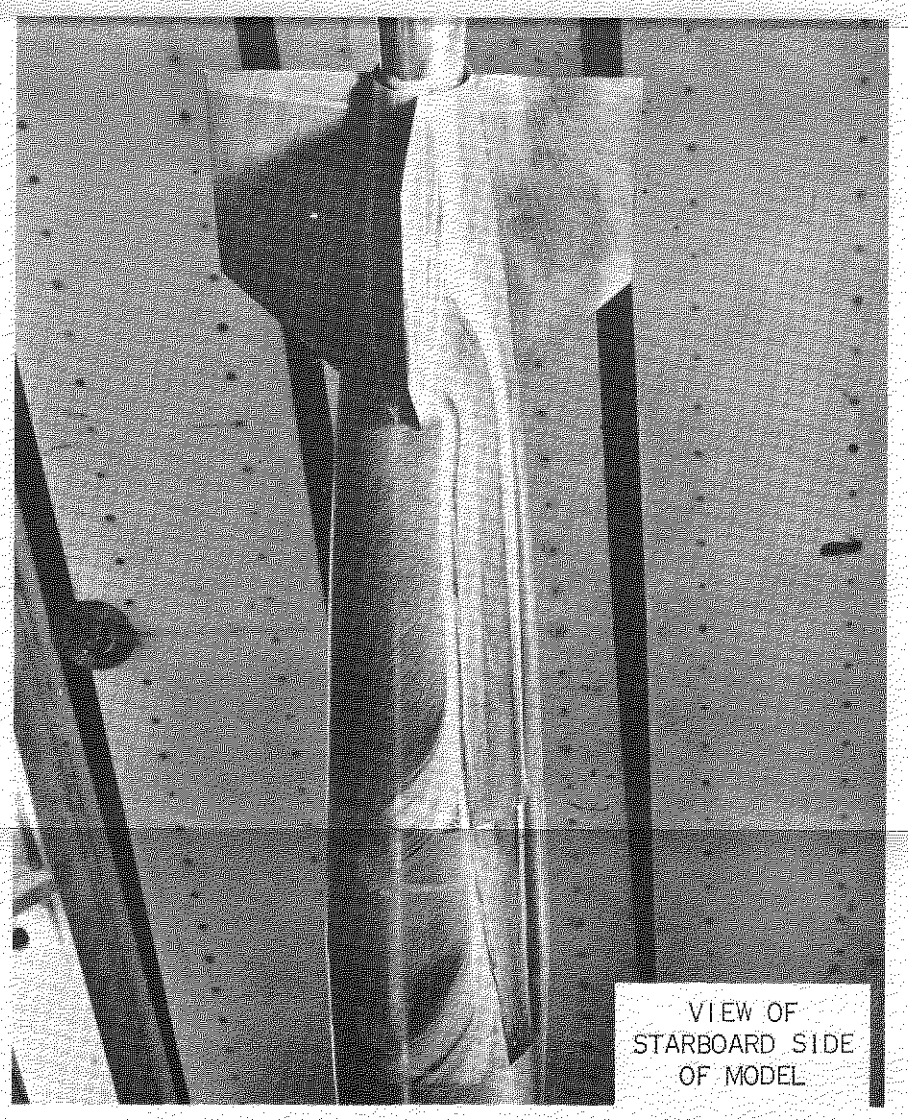

VIEW OF
STARBOARD SIDE
OF MODEL

Fig.28b. Flow visualization. Model with pointed nose (2nd series of tests)

$\sigma = 19.93^{\circ}$ $\lambda = 0^{\circ}$ $M = 0.50$ $R = 1.29 \times 10^{6}$

Printed in England for Her Majesty's Stationery Office by the Royal Aircraft Establishment, Farnborough. Dd.501871. K.4.

DETACHABLE ABSTRACT CARD

A.R C. C.P. No 1157
July 1969

Lee, P
Hacker, I G.

INDUCED ROLLING MOMENT CHARACTERISTICS OF THE M557A STREAMLINE BOMB AT MACH NUMBER 0.50

A model of a streamline bomb with fixed cruciform fins has been tested in the R A E 8 ft x 6 ft tunnel, to examine possible reasons for the discrepancy between the rolling moments derived from free flight tests and results obtained from previous wind tunnel tests

A range of Reynolds numbers was covered corresponding to the previous tunnel test and free flight values The effect on rolling moment of a nose probe and a launching lug, which were present in the flight tests but not represented in the previous tunnel tests, also was investigated

The results show that the induced rolling moment was not significantly influenced by Reynolds number, for the range covered At incidence a large change in rolling moment resulted for the addition of the nose probe and it was shown that this rolling moment depended critically on the geometric accuracy of the spherical nose of the probe itself

A.R.C. C.P. No 1157
July 1969

Lee, P
Hacker, I. G

INDUCED ROLLING MOMENT CHARACTERISTICS OF THE M557A STREAMLINE BOMB AT MACH NUMBER 0.50

A model of a streamline bomb with fixed cruciform fins has been tested in the R.A E 8 ft x 6 ft tunnel, to examine possible reasons for the discrepancy between the rolling moments derived from free flight tests and results obtained from previous wind tunnel tests.

A range of Reynolds numbers was covered corresponding to the previous tunnel test and free flight values. The effect on rolling moment of a nose probe and a launching lug, which were present in the flight tests but not represented in the previous tunnel tests, also was investigated.

The results show that the induced rolling moment was not significantly influenced by Reynolds number, for the range covered At incidence a large change in rolling moment resulted for the addition of the nose probe and it was shown that this rolling moment depended critically on the geometric accuracy of the spherical nose of the probe itself

A.R.C. C.P. No 1157
July 1969

Lee, P
Hacker, I. G

INDUCED ROLLING MOMENT CHARACTERISTICS OF THE M557A STREAMLINE BOMB AT MACH NUMBER 0.50

A model of a streamline bomb with fixed cruciform fins has been tested in the R.A.E. 8 ft x 6 ft tunnel, to examine possible reasons for the discrepancy between the rolling moments derived from free flight tests and results obtained from previous wind tunnel tests.

A range of Reynolds numbers was covered corresponding to the previous tunnel test and free flight values. The effect on rolling moment of a nose probe and a launching lug, which were present in the flight tests but not represented in the previous tunnel tests, also was investigated.

The results show that the induced rolling moment was not significantly influenced by Reynolds number, for the range covered At incidence a large change in rolling moment resulted for the addition of the nose probe and it was shown that this rolling moment depended critically on the geometric accuracy of the spherical nose of the probe itself

Published by
HER MAJESTY'S STATIONERY OFFICE

To be purchased from
49 High Holborn, London WC1 V 6HB
13a Castle Street, Edinburgh EH2 3AR
109 St Mary Street, Cardiff CF1 1JW
Brazennose Street, Manchester M60 8AS
50 Fairfax Street, Bristol BS1 3DE
258 Broad Street, Birmingham B1 2HE
80 Chichester Street, Belfast BT1 4JY
or through booksellers

C.P. No. 1157

SBN 11 470425 2